

**R.V. COLLEGE OF ENGINEERING, BENGALURU - 560059**  
**(Autonomous Institution Affiliated to VTU, BELAGAVI)**



**Power Allocation, Adaptive Beamforming in LTE  
through Pilot-Based Channel Estimation**

**PROJECT REPORT**

*Submitted by*

<b>Mohamed Omar Sharief K</b>	<b>1RV12EC089</b>
<b>Nikhil Mahadevappa Kaller</b>	<b>1RV12EC103</b>
<b>Prabhasa K</b>	<b>1RV12EC111</b>

*Under the Guidance of*

<b>Prof. Shushrutha K S</b>	<b>Dr. Saptarshi Chaudhuri</b>
<b>Assistant Professor</b>	<b>Principal Architect</b>
<b>Department of ECE</b>	<b>External Guide</b>
<b>R.V. College of Engineering</b>	<b>WIPRO, Bengaluru</b>

*In partial fulfillment for the award of degree*

*of*

*Bachelor of Engineering*

*in*

**ELECTRONICS & COMMUNICATION ENGINEERING**

**2015-2016**

**R.V. COLLEGE OF ENGINEERING, BENGALURU - 560059**  
**(Autonomous Institution Affiliated to VTU, BELAGAVI)**

**DEPARTMENT OF ELECTRONICS & COMMUNICATION ENGINEERING**



**CERTIFICATE**

This is to certify that the project work titled "**Power Allocation, Adaptive Beamforming In LTE Through Pilot-Based Channel Estimation**" is carried out by **Mohamed Omar Sharief K (1RV12EC089), Nikhil Mahadevappa Kaller (1RV12EC103), Prabhosa K (1RV12EC111)**, who are bonafide students of R.V College of Engineering, Bengaluru, in partial fulfilment for the award of degree of **Bachelor of Engineering in Electronics And Communication Department** of the **Visvesvaraya Technological University, Belagavi during the year 2015-2016**. It is certified that all corrections/suggestions indicated for the internal Assessment have been incorporated in the report submitted to the departmental library. The project report has been approved as it satisfies the academic requirements in respect of project work prescribed by the institution for the said degree.

Signature of Guide      Signature of Head of the Department      Signature of Principal

**External Viva**

**Name of Examiners**

**Signature with date**

1.

2.

**R.V. COLLEGE OF ENGINEERING, BENGALURU - 560059**  
**(Autonomous Institution Affiliated to VTU, BELAGAVI)**

**DEPARTMENT OF ELECTRONICS & COMMUNICATION ENGINEERING**

**DECLARATION**

We, **Mohamed Omar Sharief K, Nikhil Mahadevappa Kaller, Prabhosa K**, the students of eight semester B.E., Electronics and Communication Engineering, bearing USN: 1RV12EC089, 1RV12EC103, 1RV12EC111, hereby declare that the project titled "**Power Allocation, Adaptive Beamforming In LTE Through Pilot-Based Channel Estimation**" has been carried out by us and submitted in partial fulfilment for the award of degree of **Bachelor of Engineering in Electronics And Communication Department of the Visvesvaraya Technological University, Belagavi during the year 2015-2016.**

Further, we declare that the content this work has not been submitted previously by anybody for the award of degree or diploma in any other University.

**We also declare that any Intellectual Property Rights generated out of this project carried out at RVCE will be the property of R.V. College of Engineering, Bengaluru and we will be the sole authors of the same.**

Place: Bengaluru

Name

Signature

Date: 19/5/2016

MOHAMED OMAR SHARIEF K

NIKHIL MAHADEVAPPA KALLER

PRABHASA K

## **ACKNOWLEDGEMENT**

We take this opportunity to express our gratitude to the people who have been instrumental in the successful completion of this project. Apart from our efforts, the success of this project depends largely on the encouragement and guidelines of many others. It is our privilege to acknowledge many who have given a helping hand.

We are highly indebted to our External Guide, **Dr. Saptarshi Chaudhuri**, Principal Architect, WIPRO, as well as our internal guide **Prof. Shushrutha K S**, Assistant Professor, Department of Electronics and Communication Engineering, R.V. College of Engineering, Bengaluru for their timely guidance and constant supervision as well as providing necessary information and support during the entire study of the project.

We take this opportunity to thank **Dr. B. V. Uma**, Professor and Head, Department of Electronics and Communication Engineering, and **Dr. K. N. Subramanya**, Principal, R. V. College of Engineering, for their cooperation, advice and for providing this opportunity.

We would like to also thank the project staff, **Dr. Suma M. S.**, **Mrs. Saraswathi K**, **Mrs. Anusha L. S.**, Department of Electronics and Communication Engineering, R. V. College of Engineering, for their guidelines and efficient planning.

We take this opportunity to thank the internal examiners, **Dr. Uttara Kumari M** and **Dr. Veena Devi** of Dept. of Electronics and Communication Engineering and the external examiner **Dr. Uma Rao**, Professor of Department of Electrical and Electronics Engineering, R. V. College of Engineering, for their valuable suggestions.

We would like to thank the **faculty members and non-teaching staff** of Dept. of Electronics and Communication Engineering, R.V. College of Engineering for their constant support.

We like to thank our **parents and friends** for their constant moral and financial support.

## **ABSTRACT**

One of the complexities of LTE (Long Term Evolution) Wireless communication is the changing channel conditions and dynamic multi-user environment. In order to compensate for interference effects of multiple users in a cell, the system must maintain very low BER. LTE improvises on the channel coding scheme by replacing convolutional coding with a more accurate and real-time coding method. For constant monitoring of the channel condition, the Base Station and User Equipment require a reference signal through which the channel effect can be analysed, which led to the concept of Pilot-based channel estimation. Increasing customer density and usage of services demands optimised power allocation and faster scheduling of transmission. The Base Station must monitor the channel conditions each time it connects and suitably strengthen its signal, so as to effectively reach the user. This has been the motivation to incorporate power allocation and adaptive beamforming for transmission.

The work primarily involved three stages, whose sequence of operations is as follows: Recreating LTE PHY Modulation and Coding for an AWGN channel, which adaptively changes the modulation scheme and performs Turbo coding, accompanied with early termination for real-time communication, and rate matching for link adaptation. Pilot-based OFDM Channel Estimation involves sending a downlink pilot sequence, known to both base station and user equipment, through a realistic, multipath fading channel. Signals are mapped to a Resource Grid and OFDM modulated, which helps estimate the channel response. A distance based power allocation mapping is made based on the Okumura-Hata Path Loss model, following which LMS algorithm helps adaptively beam-steer the signal at the calculated power, to the user location.

The overall system block was modelled in MATLAB 2014a. The LTE-PHY downlink module was tested for Bit Error Rate (BER) under changing conditions of Signal to Noise Ratio (SNR). The communication blocks involved between the base station and the user equipment have been successfully studied and analyzed. Improvements were done on the code, with due consideration to stage-wise integration and simulation time.

## TABLE OF CONTENTS

<b>ABSTRACT .....</b>	<b>iv</b>
<b>LIST OF ABBREVIATIONS .....</b>	<b>viii</b>
<b>LIST OF TABLES.....</b>	<b>x</b>
<b>LIST OF FIGURES.....</b>	<b>xi</b>
<b>1    <i>Introduction</i> .....</b>	<b>1</b>
1.1    Key Technologies of LTE .....	3
1.2    Literature Survey.....	4
1.2.1    Pilot Based Channel Estimation.....	4
1.2.2    Power control .....	7
1.2.3    Adaptive Beamforming.....	8
1.3    Motivation .....	9
1.4    Problem Statement .....	9
1.5    Objectives.....	10
1.6    Methodology .....	10
1.7    Specifications .....	12
1.8    Organization of the report .....	14
<b>2    <i>Software Requirements</i> .....</b>	<b>15</b>
2.1    MATLAB with LTE-enabling Toolboxes.....	16
2.1.1    DSP System Toolbox .....	16
2.1.2    Communications System Toolbox .....	17
2.2    System Objects.....	17
2.2.1    Example of Communications System Toolbox .....	17
2.2.2    Functions using System Objects .....	19
2.3    Stage-wise BER Measurements .....	19
2.4    Summary .....	20
<b>3    <i>LTE-PHY Modulation and Coding</i> .....</b>	<b>21</b>
3.1    LTE Physical Layer (PHY).....	22
3.1.1    Block Diagram of LTE-PHY .....	23
3.1.2    PHY Properties .....	24
3.2    PHY Processing.....	25
3.3    Modulation and Coding.....	26

3.3.1	Modulation Schemes.....	27
3.3.2	Demodulation.....	30
3.3.3	Scrambling .....	31
3.3.4	Turbo Coding .....	33
3.3.5	Early termination mechanism .....	34
3.3.6	Algorithm for Rate Matching.....	35
3.3.7	Channel Processing.....	36
3.4	Summary .....	37
<b>4</b>	<b>Pilot-based OFDM Channel Estimation .....</b>	<b>38</b>
4.1	Realistic Channels .....	40
4.1.1	Multipath Fading.....	40
4.1.2	Doppler Effects .....	41
4.1.3	MATLAB Tools for realistic channels .....	41
4.2	Configuring the LTE Resource Grid.....	42
4.2.1	CSR Symbols – Pilot Signals.....	42
4.3	Pilot Signal Generation .....	44
4.4	Resource Element Mapping .....	46
4.5	OFDM Signal Generation .....	47
4.5.1	Channel Modeling.....	47
4.6	Inverse Operations at Receiver end.....	48
4.7	Channel Estimation .....	49
4.7.1	Interpolation.....	49
4.7.2	Equalizer Gain Computation.....	50
4.8	Summary .....	51
<b>5</b>	<b>Power Allocation and Beamforming .....</b>	<b>52</b>
5.1	Path Loss Modeling.....	53
5.1.1	Free space equations .....	53
5.1.2	Wireless medium equations .....	54
5.1.3	Okumura Hata model.....	55
5.1.4	Path Loss Model for LTE .....	56
5.2	Power Control .....	57
5.2.1	Distance Based Power allocation algorithm .....	57
5.2.2	Power Control in LTE.....	59
5.2.3	Downlink Power Allocation .....	60

5.2.4	Mapping CQI, SNR with distance .....	60
5.3	LMS Adaptive Beamforming.....	63
5.4	Summary .....	67
<b>6</b>	<b><i>Conclusion</i></b> .....	<b>68</b>
6.1	Work Done .....	69
6.2	Future Scope.....	69
6.3	Learnings from the Project.....	70
	<b>REFERENCES</b> .....	<b>71</b>
	<b>APPENDIX – RESOURCE GRID CONFIGURATION</b> .....	<b>76</b>

## LIST OF ABBREVIATIONS

BCH	Broadcast Channel
BER	Bit Error Rate
CP	Cyclic Prefix
CQI	Channel Quality Indicator
CRC	Cyclic Redundancy Check
CSI	Channel State Information
CSR	Cell-Specific Reference
DSP	Digital Signal Processing
eNodeB	evolved Node B
EPRE	Energy Per Resource Element
FDD	Frequency Division Duplex
LTE	Long Term Evolution
MAC	Medium Access Control
MIMO	Multiple Input Multiple Output
MMSE	Minimum Mean Square Error
MRC	Maximum Ratio Combining
MU-MIMO	Multi-User Multiple Input Multiple Output
OFDM	Orthogonal Frequency Division Multiplexing
PBCH	Physical Broadcast Channel
PDCCH	Physical Downlink Control Channel
PDSCH	Physical Downlink Shared Channel
PHY	Physical Layer
PRBs	Physical Resource Blocks
PSS	Primary Synchronization Signal
QAM	Quadrature Amplitude Modulation
QoS	Quality of Service
QPSK	Quadrature Phase Shift Keying
RLC	Radio Link Control
RRC	Radio Resource Control
RRM	Radio Resource Management
SC-FDM	Single-Carrier Frequency Division Multiplexing
SIR	Signal-to-Interference Ratio

SINR	Signal-to-Interference-plus-Noise Ratio
SNR	Signal-to-Noise Ratio
SSS	Secondary Synchronization Signal
TPC	Transmit Power Control
UE	User Equipment
ZF	Zero Forcing

## LIST OF TABLES

<b>Table 1.1</b> LTE Specifications.....	12
<b>Table 1.2</b> Project Specifications .....	13
<b>Table 2.1</b> QPSK Transceiver.....	19
<b>Table 3.1</b> BER calculation functions.....	26
<b>Table 3.2</b> Modulator function.....	29
<b>Table 3.3</b> Demodulator function .....	31
<b>Table 3.4</b> Scrambler function .....	32
<b>Table 3.5</b> Descrambler function .....	32
<b>Table 3.6</b> Turbo-Encoder function .....	34
<b>Table 3.7</b> Early termination function .....	35
<b>Table 3.8</b> Rate Matching function.....	36
<b>Table 4.1</b> Resource Grid Configuration .....	42
<b>Table 4.2</b> Pilot Signal Generation .....	44
<b>Table 4.3</b> Resource Element Mapping .....	45
<b>Table 4.4</b> OFDM Signal Generation .....	47
<b>Table 4.5</b> Channel Modelling.....	47
<b>Table 4.6</b> OFDM Signal Reception.....	48
<b>Table 4.7</b> Channel Estimation Function.....	49
<b>Table 4.8</b> Interpolation Function .....	50
<b>Table 4.9</b> Equalizer Gain Computation .....	50
<b>Table 5.1</b> Valid parameters range of the Okumura Hata model.....	55
<b>Table 5.2</b> CQI Index .....	61

## LIST OF FIGURES

<b>Fig. 1.1</b> Wireless Standards Evolution [1].....	2
<b>Fig. 1.2</b> LTE Nomenclature .....	3
<b>Fig. 1.3</b> System Block Diagram.....	9
<b>Fig. 1.4</b> Modulation and Coding blocks – Chapter 3.....	10
<b>Fig. 1.5</b> Pilot Symbol Generation – Chapter 4.....	11
<b>Fig. 1.6</b> Channel Estimation – Chapter 4.....	11
<b>Fig. 2.1</b> BER vs SNR of QPSK Modulator as a system object .....	20
<b>Fig. 3.1</b> LTE network architecture [1] .....	22
<b>Fig. 3.2</b> Physical layer specifications in Downlink LTE [1] .....	23
<b>Fig. 3.3</b> LTE time-domain structure [1].....	25
<b>Fig. 3.4</b> Mapping LTE downlink logical, transport, and physical channels .....	25
<b>Fig. 3.5</b> Constellation diagram of A – QPSK, B – 16-QAM, C – 64-QAM .....	30
<b>Fig. 3.6</b> BER vs SNR plot – Modulation-Demodulation.....	31
<b>Fig. 3.7</b> BER vs SNR plot – Scrambling-Descrambling .....	32
<b>Fig. 3.8</b> Block diagram of a turbo encoder .....	33
<b>Fig. 3.9</b> BER vs SNR plot –Turbo Encoder-Decoder.....	34
<b>Fig. 3.10</b> Comparison of Turbo Coding, without and with Early Termination .....	35
<b>Fig. 3.11</b> BER vs SNR plot for 1/3 and 1/2 rate .....	36
<b>Fig. 4.1</b> Physical layer specifications in Downlink LTE [1] .....	39
<b>Fig. 4.2</b> LTE resource grid content [1] .....	41
<b>Fig. 4.3</b> Signal content of LTE downlink subframe [1].....	43
<b>Fig. 4.4</b> LTE resource grid configuration: Parameter variation for different Bandwidths .....	43
<b>Fig. 4.5</b> LTE resource grid configuration: fixed BW, Varying Modulation Scheme (QPSK, 16-QAM) .....	44
<b>Fig. 4.6</b> LTE resource grid configuration: Varying BW (1.4, 3, 5, 10 MHz) Fixed Modulation Scheme .....	45
<b>Fig. 4.7</b> Pilot Signal Generation .....	46
<b>Fig. 4.8</b> Received Resource Grid .....	48
<b>Fig. 4.9</b> Equalized Resource Grid.....	51
<b>Fig. 4.10</b> Completed Blocks .....	51
<b>Fig. 5.1</b> Okumura Hata Model .....	56

<b>Fig. 5.2</b> Okumura Hata Model for LTE .....	57
<b>Fig. 5.3</b> Outage Percentage of Mobiles in Outage versus No .of Mobiles in Cell .....	59
<b>Fig. 5.4</b> Simulation for eNodeB = 1 and UE = 5 .....	62
<b>Fig. 5.5</b> Mapping CQI, SNR with distance to eNodeB .....	62
<b>Fig. 5.6</b> LMS Algorithm .....	63
<b>Fig. 5.7</b> A - Amplitude pattern, B – Polar Pattern for 5 antenna system.....	65
<b>Fig. 5.8</b> Same Parameter values with number of antennas increased from 5 to 10 .....	66

*Chapter 1*

*Introduction*

# CHAPTER 1

## INTRODUCTION

The rapid surge in mobile services and data intensive applications like browsing, social networking, and video streaming has become a major driving force for the development of wireless standards. LTE (Long Term Evolution) and LTE-Advanced are the latest mobile communications standards developed by the Third Generation Partnership Project (3GPP), in order to meet the above requirements. LTE standardization was announced to the world in 2008, which has now evolved into LTE-Advanced, bringing in improvements in data rates and user experience. Fig. 1.1 shows the evolution in Wireless Standards.

The goals and objectives of LTE and LTE-Advanced include enhanced radio access rates, improvement in capacity, coverage, and spectral efficiency, flexible bandwidth operations, low latency, reduced operation and maintenance costs, multi-antenna support, and smooth integration with the Internet and existing mobile telecommunication systems.

Successful data transmission must happen under dynamic radio channel conditions and taking user mobility into account. LTE thus brings in smart antenna, MIMO technologies. Adaptive beamforming, and its necessary prerequisites are the factors addressed in this project.

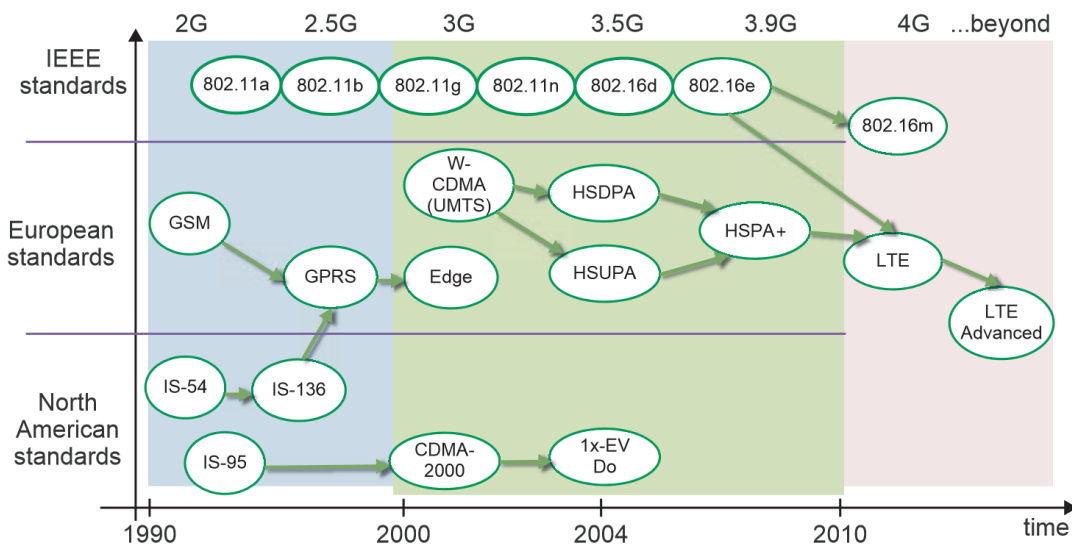


**Fig. 1.1** Wireless Standards Evolution [1]

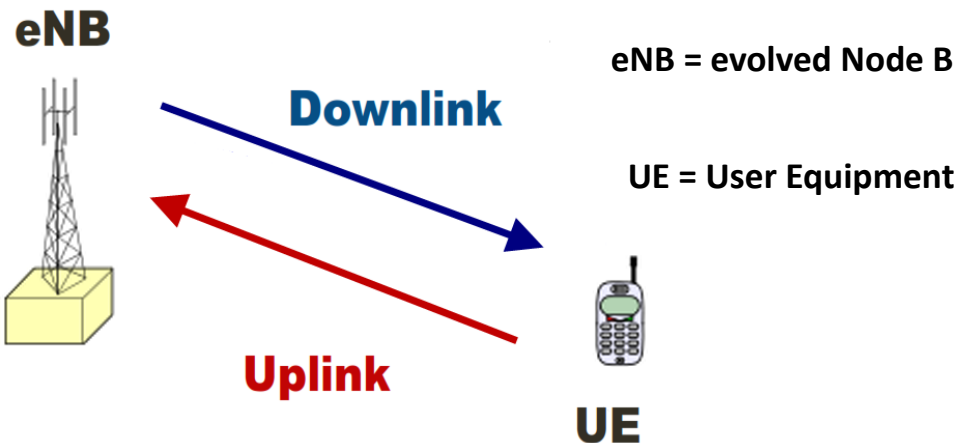


**Fig. 1.2** LTE Nomenclature

In 3GPP nomenclature, shown in Fig. 1.2, the mobile unit is termed as UE (User Equipment) whereas the base station is called as eNodeB (evolved Node B). Data transmission from eNodeB to UE is referred to as a Downlink operation, and vice-versa. The entire project involves LTE Downlink transmission scheme.

## 1.1 Key Technologies of LTE

The LTE enabling technologies, and what makes it so attractive as compared to the remaining standards, include the following:

1. **Downlink OFDM:** The primary idea in OFDM is to divide the data transmitted on a channel in the frequency domain and to arrange the symbols with multiple subcarriers. The main reasons LTE selects OFDM as the basic transmission scheme is its robustness to high spectral efficiency, multipath fading channel supports frequency-selective scheduling, low-complexity implementation, MIMO transmission, and interference coordination. OFDM estimates the channel frequency response in a simple and intuitive method, based on pilot signals. With an accurate estimate of the receiver channel response, the best replica of the transmitted signal can be recovered using an equalizer.
2. **Uplink SC-FDM:** The huge variations in the transmit power hugely affect the Uplink operation, resulting in efficiency reduction of UE power consumption. The design of complex power amplifiers is a tough task especially for uplink transmission. Thus, uplink transmission uses SC-FDM.

3. **MIMO:** Apart from increase in demand for more bandwidth, the cellularization, sectorization and the improvement in air interface capabilities, the performance enhancement of wireless systems' can be done with the help of smart antennas, which is the concept behind MIMO. MIMO for LTE can be categorized into the following areas: transmit and receive diversity, adaptive beamforming, and importantly spatial multiplexing. The data rates can be improvement is directly proportional to the number of transmitter antennas.
4. **Evolution of Channel Coding:** Unlike Convolutional coding, which was used in all previous standards, LTE has introduced Turbo Coding. They aim at increasing efficiency, by using an early termination mechanism, which depends on code quality. Instead of completing all iterations, the decoding can be terminated if there is no CRC error.
5. **Channel-dependent Scheduling and Link Adaptation:** Link adaptation involves altering and adapting the properties of a mobile communication system to respond to the dynamic nature of the channel. Different modulation schemes and coding techniques can be applied, number of transmit and receive antennas and bandwidth changed, depending on the channel quality at that instant. Channel-dependent scheduling caters to as many users in the range, while ensuring the best quality-of-service levels based on the existing instantaneous channel condition.

## 1.2 Literature Survey

This survey has been organized in three parts, and is as follows:

1. Pilot Based Channel Estimation
2. Power Control
3. Adaptive Beamforming

### 1.2.1 Pilot Based Channel Estimation

OFDM is fast gaining popularity in modern communication systems due to its ability to transmit high amount of data at comparatively slower symbol rates and its favourable

performance in presence of fading. Usage of OFDM has been proposed for 4G mobile communication and several IEEE communication standards. For the design of a channel estimator in OFDM systems, insertion of pilot signals prove vital. Pilot signals are reference signals that are inserted into the payload and are used by both transmitters and receivers. There are two types of pilots - block type and comb type.

A robust beam-forming for the adaptive antenna array of base station is proposed in reference [1, 2] with the help of orthogonal pilot signals. It demonstrates that the channel response can be accurately estimated using a finite length spread sequence.

Alexander Seeger et.al explains a novel method to achieve both beamforming gain and diversity gain by means of a feedback of downlink characteristics from eNodeB to UE in reference [3]. The paper aims at reducing effect of feedback errors by a scheme called antenna weight verification which increases the accuracy of estimation and reduces errors.

Shirish Nagaraj and Yih-Fang Huang propose a channel estimation scheme that is based on channel state information in [4, 5]. The proposed system was used to adaptively estimate the downlink fading channel at the base station. The most optimal mode of transmission can be determined from the channel co-efficients. The channel estimation requires calculation at the mobile end by receiving the pilot signal. The simulations show considerable improvement in beamforming gains with the addition of feedback scheme.

The effect of inaccurate channel state information is analysed in [6, 7] in terms of average bit error probability, spectral efficiency and outage probability on transmit beamforming over MIMO Rayleigh channels using pilot modulation. Inaccurate CSI accounts for estimation, prediction errors leading to mismatch in beamforming weights.

Channel estimation proposed exploits the control area channel estimation for LTE downlink in [8, 9]. The LTE standards adopt training data known as cell specific reference signals to estimate channel response accurately. Due to very high accuracy of control area channel estimation, the output of control area channel is used as a virtual pilot to estimate the channel response.

A new pilot-aided algorithm for the estimation of fast time-varying channels in OFDM transmission is proposed in reference [13, 14]. Unlike many existing OFDM channel estimation algorithms in the literature, it proposes to perform channel estimation in the

frequency domain, to exploit the structure of the channel response, optimize the pilot group size and perform most of the computations offline resulting in high performance at substantial complexity reductions.

The use of decision directed (DD) channel estimation in a multiple-input multiple-output (MIMO) orthogonal frequency division multiplexing (OFDM) downlink receiver is studied in reference [15]. The 3GPP LTE based pilot structure is used as a benchmark. The space-alternating generalized expectation-maximization (SAGE) algorithm is used to improve the performance from that of the pilot symbol based least-squares (LS) channel estimator.

An enhanced DFT-based channel estimation technique for the long term evolution (LTE) based cellular uplink is proposed in [16]. A sinc-null based noise power estimation method in conjunction with a dynamic noise removal technique is proposed to suppress the noise in the time domain and achieve better performance while keeping the complexity in check.

The channel estimation algorithms for the downlink of 3GPP LTE systems is compared in reference [17]. This helped us decide on the algorithm.

An enhanced channel estimation method for multi-user multiple-input multiple output (MU-MIMO) based long term evolution (LTE)-Advanced system is presented in [18]. The proposed method partially estimates and eliminates the multi-user interference using a simple pilot matrix inversion based scheme. A channel estimation scheme with adaptive noise and interference weighting method to increase the estimation accuracy is applied.

The LTE channel estimation algorithm based on the pilot location is studied in reference [19]. According to the disadvantage of large computation and complexity about MMSE, a simplified algorithm based on singular value decomposition SVD is used to reduce the operation complexity.

The channel estimation and data detection for Long Term Evolution (LTE) air interface over time varying frequency selective channels using a modified superimposed training (SIT) sequence method are discussed in [20]. This method can be significantly improved the accuracy by exploiting time and frequency correlations between the channel frequency response coefficients (coherence time and coherence bandwidth).

### 1.2.2 Power control

An enhanced closed loop power control technique for UTRA TDD, which adapts the step size according to relative path loss (or power) measurements at the transmitter side is proposed in [21]. It shows that the link-level performance of the proposed power control can be significantly better than the existing closed loop power control. The largest gains are obtained for slow and moderate fading channels.

The performance of 3GPP Long Term Evolution (LTE) closed loop power control combined with fractional path loss compensation factor is evaluated by simulating the effects of open loop error, Transmit Power Control (TPC) command delay and power headroom reporting in reference [22]. It shows that the closed loop power control with fractional path loss compensation factor is advantageous compared to closed loop power control with full path loss compensation.

The system performance of a truncated closed-loop power-control (TCPC) scheme for uplinks in direct-sequence/code-division multiple-access cellular systems over frequency-selective fading channels has been analyzed in [23]. In this TCPC scheme, a mobile station (MS) suspends its transmission when the short-term fading is less than a preset cutoff threshold; otherwise, the MS transmits with power adapted to compensate for the short-term fading so that the received signal power level remains constant.

A new variable step closed-loop power control algorithm (VSPC) and fixed-step closed loop power control with information feedback (FSPC-IF), that are able to increase speed of convergence and alleviate the effect of the loop delay have been presented in [24].

The difference in performance between pure open-loop and combined open and closed-loop power control has been analyzed in [25] and the different behavior of fractional vs. full path-loss compensation has been evaluated. It demonstrates the effect of distance path-loss of a test user on several physical layer performance metrics including throughput, resource allocation as well as modulation and coding scheme utilization.

A feasible UL power control mechanism is proposed in [26] to manage eNB-to-eNB interference, where different UL power control parameters are set based on different interference level.

Arne Simonsson presents the 3GPP long term evolution (LTE) power control mechanism, and compares its performance to two reference mechanisms in [27]. The LTE power control mechanism constitutes of a closed loop component operating around an open loop point of operation. Specifically, the open loop component has a parameterized fractional path loss compensation factor, enabling a trade-off between cell edge bitrate and cell capacity. The closed-loop component can be limited to compensate for long-term variations, enabling fast channel quality variations to be utilized by scheduling and link adaptation.

Resource scheduling algorithm with power control technique is proposed in [28], which considers channel characteristics and minimum power requirement at the base station for successful reception of a signal.

### **1.2.3 Adaptive Beamforming**

Beamforming uses antenna arrays to concentrate energy in a particular direction, increasing directivity and also reducing interference. 3GPP LTE and LTE-Advanced have introduced MIMO to improve spectral efficiency. E.M. Al-Ardi et al in [29] performs an evaluation of the Least Mean Square algorithm in adaptive beamforming. The evaluation takes into consideration the number of elements in the array, physical spacing between them, number of signals incident and their angular separation. A new technique to mitigate the inter cell interference for cell edge users in LTE-A system with adaptive beamforming technique is introduced in reference [30].

Antenna arrays facilitate MIMO by efficiently using both the elevation and azimuthal domain as explained in [31]. [32, 33] also explains the way in which antenna arrays provide additional degrees of freedom. The adaptive antenna array system comprises of transceiver unit, radio distribution network and antenna array unit [35]. The transceiver can be considered as a set of logical antenna ports. The transceiver signal is delivered to the antenna elements from the radio distribution network. Transceivers can be configured adaptively to multiplex a number of users [5]. It also suggests the use of pilot signals to determine the channel state information (CSI). [6] Investigates the channel characteristics in presence of different configurations of antenna array systems.

### 1.3 Motivation

The number of mobile phone users has grown rapidly worldwide in recent years. Moreover, these users have increased their demand on bandwidth and quality of services. For this reason the existing technologies must be continually improved to meet in fast and adequate market demand. On the other hand in order to offer bigger capacity to the users the operators require technologies more efficient in the use of resources to reduce costs. The LTE network platform is able to deliver best mobile broadband services to the customer that can support the fast growth rate of subscriber including with high data rates. But it suffers from problems such as interference, constantly varying channel conditions, fading (both large scale and small scale) and power allocation. These problems are to be tackled efficiently while ensuring the adequate quality of service levels. The need of the hour is also to take into consideration fading effects, power requirements and dynamicity of the channel as well as of the user. These all worked as a motivation for this project.

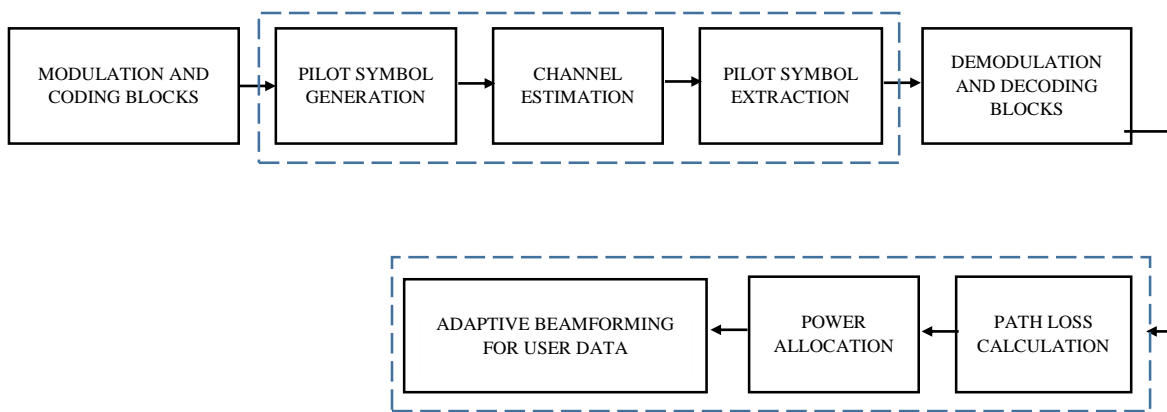


**Fig. 1.3 System Block Diagram**

### 1.4 Problem Statement

Wireless communication in LTE involves multi-user, fading environment, with dynamic channel conditions. This requires that the eNodeB antennas must:

- Adaptively steer the signal to the User Equipment
- With a suitable power
- Based on real-time channel conditions

This project addresses the above requirements by simulating Pilot-based downlink channel estimation, Okumura-Hata path loss model, distance-based power allocation and LMS adaptive beamforming in MATLAB.

## 1.5 Objectives

For the successful completion of this project, the objectives that were met are as follows

1. Understanding of LTE-PHY and its enabling technologies such as OFDM, Transmit Diversity, Adaptive modulation
2. Recreate LTE PHY modules that implement LTE-specific Modulation and Coding
3. Pilot-based downlink OFDM Channel Estimation techniques, incorporating multipath fading and Doppler effects
4. Path Loss calculation and Distance Based Power allocation for mapping UE location and Power required, LMS Adaptive beam-steering through eNodeB antenna array

## 1.6 Methodology

To maintain connection between the UE and eNodeB antennas during data transmission, channel has to be monitored and suitable power needs to be allocated to each user. The project can be divided into blocks as shown in Fig. 1.3, each of which is mapped to the Chapter as mentioned under motivation. Each block comprises of multiple modules, with the sequence of operations as follows:

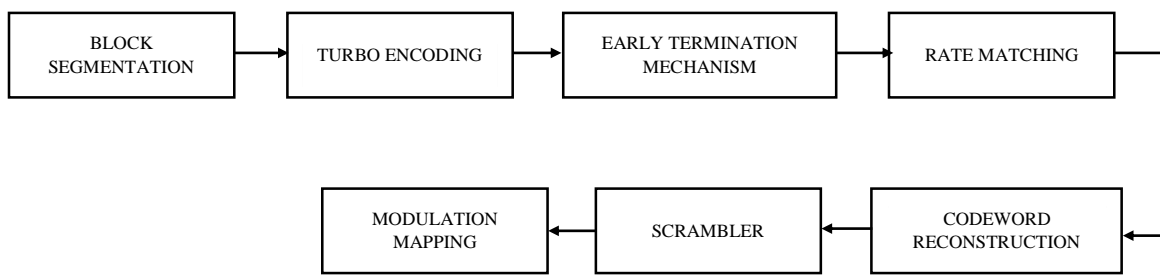


**Fig. 1.4** Modulation and Coding blocks – Chapter 3

One of the complexities of mobile communication is the dynamic conditions of the user equipment and the channel. Since the number of users in a cell might vary, the system must maintain very low BER. Modulation and Coding schemes specific to LTE were realised

for an AWGN Channel, with each component's contribution validated through BER vs SNR plots. The block included adaptive modulation, scrambling, Turbo Coding, accompanied with early termination for real-time communication and rate matching for link adaptation (Chapter 3).

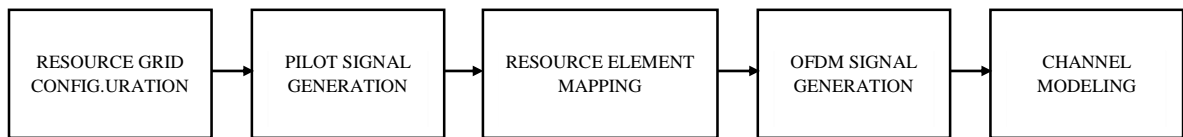


**Fig. 1.5** Pilot Symbol Generation – Chapter 4

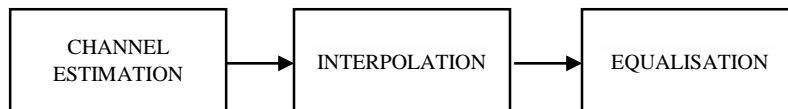


**Fig. 1.6** Channel Estimation – Chapter 4

For constant monitoring of the channel condition, eNodeB and UE require a reference signal through which the channel effect can be felt at both ends. This led to the concept of Pilot-based channel estimation. Modulation and coding performed for an AWGN Channel was extended to a realistic, fading OFDM channel. Resource Grid configuration, pilot signal generation, element mapping are the stages involved. (Chapter 4).

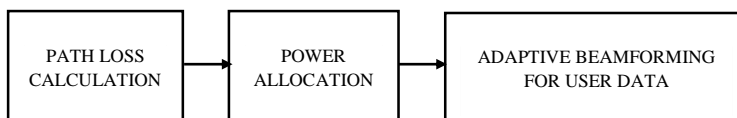


**Fig. 1.7** Power Control and beamforming – Chapter 5

Increasing customer density and usage demands faster scheduling of transmission. eNodeB must monitor the channel conditions each time it connects and suitably strengthen its signal, so as to effectively reach the user. Okumura-Hata Path Loss calculation determines the minimum amount of power to be transmitted to the UE for proper reception of signal. Distance Based Power control provides a CQI through which UE distance from the eNodeB can be mapped to evaluate Power allocation. The eNodeB signal is finally sent to the UE location by performing LMS Adaptive beam-steering, nulling the signal in the direction of interferers, i.e. other UEs. (Chapter 5).

## 1.7 Specifications

3GPP has released the 36-series of specifications specifically for LTE, LTE-Advanced radio technology. The series contains 237 specifications. Table 1.1 provides a list of specifications that hold relevance to the project.

Table 1.2 gives a list of LTE PHY Downlink, block diagram specifications used in the project. Some parameters like Frequency range, Subcarrier spacing, Modulation Schemes etc. are standardized by 3GPP.

**Table 1.1** LTE Specifications

Specification No.	Description
TS 36.101	User Equipment (UE) radio transmission and reception
TS 36.104	Base Station (eNodeB) radio transmission and reception
TS 36.201	LTE physical layer: General description
TS 36.211	Physical channels and modulation
TS 36.212	Multiplexing and channel coding
TS 36.213	Physical layer procedures
TS 36.214	Physical layer measurements
TS 36.305	Functional specification of User Equipment (UE) positioning
TR 36.824	LTE coverage enhancements
TR 36.863	Study on Cell-specific Reference Signals (CRS)
TR 36.897	Study on Elevation Beamforming for LTE

**Table 1.2** Project Specifications

Sl No	Parameter	Specifications
1	LTE Version	Release 8
2	Layer involved	LTE PHY – Layer 1
3	Mode and Duplexing	Downlink, FDD
4	Frequency Bands	25 for FDD, 11 for TDD
5	Frequency range	1.9 GHz to 3.8 GHz
6	Subcarrier spacing	15kHz
7	Channel Bandwidth (LTE specified)	1.4-20 MHz
8	Number of Resource Blocks (Depends on BW)	6-100
9	Subcarrier per Resource Block	12
10	OFDM symbols per Resource Block	7
11	Types of Channel Information	6
Sl No	Block	Specifications
1	Modulator/Demodulator (Adaptive)	QPSK, 16-QAM, 64-QAM
2	Scrambler/Descrambler	Number of shift registers:31
3	Turbo Encoder/Decoder	Rate: 1/3, Block Size: 40-6144
4	CRC Generator/Detector	Length: 24 bits
5	FFT (Block size depends on Bandwidth used)	Size: 128-2048

## 1.8 Organization of the report

In each chapter, blocks are modelled in MATLAB that iteratively and progressively build up components of the LTE PHY.

**Chapter 1** explains the need for LTE, Adaptive Beamforming, and Power Control. Problem Statement, Motivation, Methodology, Block Diagram, Specifications, and organisation of the project have been discussed.

**Chapter 2** is an insight into the numerous tools and features of MATLAB: Toolboxes and System Objects, which are used for the modelling and simulation of LTE PHY blocks.

**Chapter 3** implements LTE PHY downlink model as per the standard. It is modelled in MATLAB to obtain stage-wise results of modulation and coding techniques, assuming an AWGN Channel. BER versus SNR plots are used for performance analysis.

**Chapter 4** considers a realistic, fading channel to realise pilot-based OFDM Channel Estimation. Resource signal generation, Element Mapping, Grid configuration, OFDM signal transmission, Channel Response Estimation, Equalization are the sections involved.

**Chapter 5** describes operations performed on the estimated channel to evaluate the power required by a user, at a particular distance from the eNodeB. Okumura-Hata Path Loss modelling, distance-based power allocation, LMS adaptive beamforming are simulated using results from previous chapters.

**Chapter 6** gives a summary of the work and concludes the project. Future work, possible developments and learning outcomes have been discussed.

*Chapter 2*  
*Software Requirements*

## CHAPTER 2

### SOFTWARE REQUIREMENTS

MATLAB is a widely-used and popular platform for algorithm development, data analysis, numerical computation, and visualization.

Section 2.1 introduces the primary enabling modules for LTE PHY simulation. Section 2.2 shows how system objects help write MATLAB scripts at every stage. Section 2.3 illustrates performance measures such as BER versus SNR that have been plotted to ensure proper modelling of blocks. Programs for the entire block diagram, specified as per standard, has been successfully written and verified, as explained in Section 2.4.

#### **2.1 MATLAB with LTE-enabling Toolboxes**

MATLAB's additional plugin-like software kits are called toolboxes. They offer specific mathematical functionalities, particularly in the fields of signal processing and communications. They supplement the basic MATLAB library and offer functions that are application-specific and objects that help accelerate the procedure of developing and making algorithms and systems. These algorithmic in-built utilities help us concentrate on our area of application rather than the need to re-implement the basics.

Two system toolboxes – DSP System Toolbox [32], Communications System Toolbox [33], are particularly helpful for LTE PHY simulation.

##### **2.1.1 DSP System Toolbox**

The DSP System Toolbox gives inbuilt functionality for algorithms and tools that perform basic signal processing. It includes a host of specialized filter design capabilities, FFTs (Fast Fourier Transforms), and algorithms built in as System objects that make the job of processing information and creating real-time archetypes easier. It contains tools for that perform specific functions like connecting to audio files and devices, performing spectral analysis, and using interactive visualization techniques that allow the user to analyze system behavior and performance. All these modules support C/C++ code production automatically; most also support fixed-point data, and a few allow generation of HDL code.

### 2.1.2 Communications System Toolbox

The Communications System Toolbox offers tools and algorithms for the design, simulation, and evaluation of communications systems. This has specific designs for the modeling of the PHY of communications systems. It has documentation and functionality for modules like those for source coding, channel, channel coding, interleaving, modulation, equalization, synchronization, MIMO, and channel modelling, that are provided as MATLAB functions, system objects, and Simulink blocks, so that they can be used as part of system models. It also supports C/C++ code creation in the form of ‘MATLAB Coder’.

## 2.2 System Objects

System objects are a very useful, easy and convenient way of expressing communications systems and they make the developed MATLAB programs more comprehensible and sharable. They are MATLAB objects that denote time-based and executable algorithms and are organized as objects to make them simpler to use and virtually self-documenting.

### 2.2.1 Example of Communications System Toolbox

The comm or communication package of the Communications System Toolbox contains System objects and their names begin with the general prefix “comm.” The following command needs to be typed at the MATLAB command prompt to access all of the System objects of the Communications System Toolbox:

```
>> comm.<Tab>
```

The command results in an alphabetically ordered list of all the System objects existing in the toolbox. In the latest release of MATLAB (version 2015b), the Communications System Toolbox comprises a total of 123 algorithms offered as System objects.

Every System object has two parameters: properties and methods. Default properties appear when they are created. By looking at the property list of a given System object, the parameters it can take and the values normally allocated to them can be found out.

The step command is the main method of execution of a System object. Once an object is created and configured, inputs can be passed and its step method can be called to generate outputs.

The starting point for using MATLAB in this project was through the system object *comm.QPSKModulator*, whose instance was created. The following procedure was used to understand QPSK Modulator, and can be generalized to any system object:

1. Look for the system object in the command window

*>> helpwin comm.QPSKModulator*

2. Syntax for creating the system object

*H = comm.QPSKModulator* creates a modulator System object, H. This object modulates the input signal using the quadrature phase shift keying (QPSK) method.

*H = comm.QPSKModulator(Name,Value)* creates a QPSK modulator object, H, with the specified property ‘Name’ set to the specified ‘Value’.

3. Step method syntax:

*Y = step(H,X)* modulates input data, X, with the QPSK modulator System object, H. It returns the baseband modulated output, Y.

4. QPSKModulator properties:

- *PhaseOffset* - Phase of zeroth point of constellation
- *BitInput* - Assume bit inputs
- *SymbolMapping* - Constellation encoding
- *OutputDataType* - Data type of output

The MATLAB code for using the above system object is as shown below:

```
data = randi([0 1],96,1);  
hModulator = comm.QPSKModulator('BitInput',true);  
hModulator.PhaseOffset = pi/16;  
modData = step(hModulator, data);  
scatterplot(modData)
```

### 2.2.2 Functions using System Objects

A MATLAB function is written that represents a QPSK transceiver block. This function takes three inputs. The code processes each  $E_b/N_0$  value by running it in a while loop until either the specified maximum number of errors is observed or the maximum number of bits is processed. It computes two outputs, whose plot is shown in Fig. 2.1

**Table 2.1** QPSK Transceiver

SL NO	FUNCTION INPUT PARAMETERS	FUNCTION OUTPUT	SYSTEM OBJECTS USED
1	$E_b/N_0$ value	Bit Error Rate	comm.QPSKModulator
2	Limit on maximum number of errors	Number of bits processed	comm.QPSKDmodulator
3	Limit on maximum number of bits processed		comm.AWGNChannel

### 2.3 Stage-wise BER Measurements

Every section in the LTE PHY block will undergo performance analysis in terms of BER vs SNR measurements. Listed in Table 2.1, the function is a part of the ‘main’ program, which will be iterated to obtain plots for varying SNR values.

The system object that helped in modelling the realistic, multipath fading channel, *comm.LTEMIMOChannel*, has the following properties:

1. *SampleRate* - Input signal sample rate (Hz)
2. *Profile* - Channel propagation profile
3. *AntennaConfiguration* - Antenna configuration
4. *CorrelationLevel* - Spatial correlation strength
5. *AntennaSelection* - Optional transmit and/or receive antenna selection
6. *RandomStream* - Source of random number stream
7. *NormalizePathGains* - Normalize path gains
8. *NormalizeChannelOutputs* - Normalize channel outputs
9. *PathGainsOutputPort* - Enable path gain output

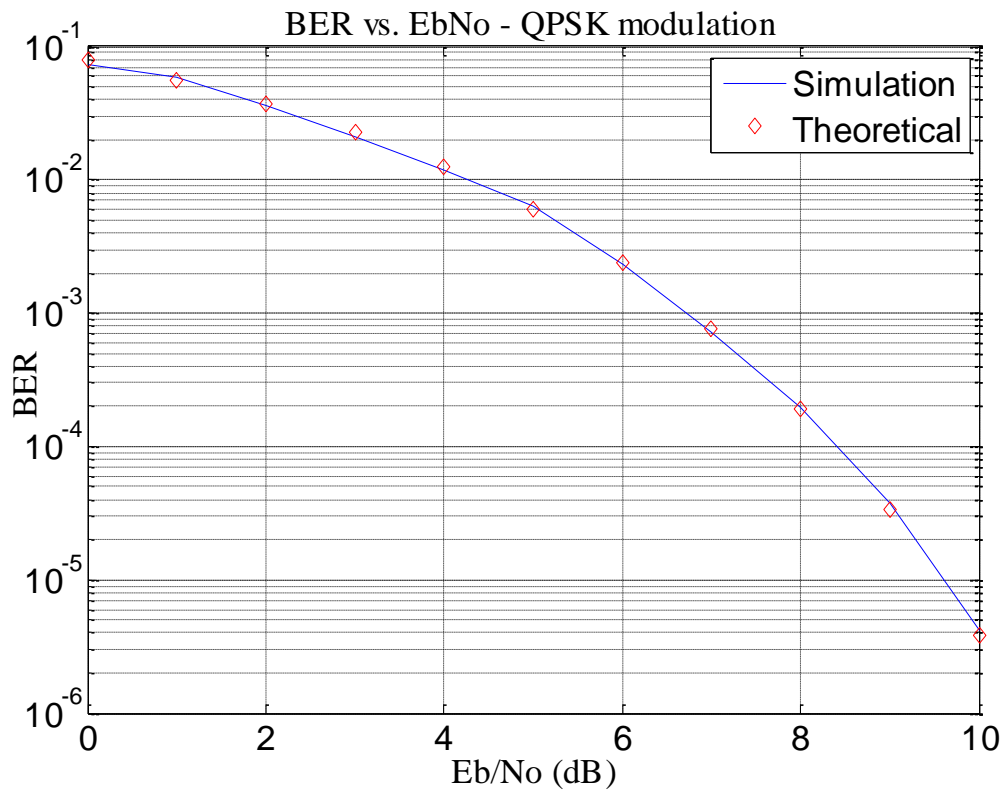


Fig. 2.1 BER vs SNR of QPSK Modulator as a system object

## 2.4 Summary

In this Chapter, simulation of a simple communication channel setup has been successfully verified. For each component progressively added, the BER reduced, for a given value of SNR. All the blocks were tested through a random input generated by MATLAB and passing it throughout the chain of both transmitter, receiver blocks. If the input was same as the output, then it was confirmed that the blocks are functioning as prescribed.

Inclusion of System Objects has greatly helped in easy verification of each progressively added block, owing to its property of repeatability. MATLAB version 2014a has been used, so as to utilise the latest toolboxes related to LTE. The next chapter primarily deals with an LTE-based modulation and coding scheme which helps pass data through an AWGN channel.

*Chapter 3*

***LTE-PHY Modulation and Coding***

## CHAPTER 3

### LTE-PHY MODULATION AND CODING

Modulation and coding at the transmitter, along with their reverse operations, namely demodulation and decoding at the receiver are the primary blocks of any wireless communication system. In this chapter, Signal Processing of LTE Physical Layer (LTE PHY) will be dealt with, as explained in Section 3.1 and 3.2.

Section 3.3 is organised as follows. Three modulation schemes are adaptively used in the case of LTE, which changes depending on the user distance from eNodeB. The coding block involves scrambling, turbo coding, early termination mechanism, rate matching and codeword reconstruction. All the blocks were simulated in MATLAB, BER vs SNR plots verified. All this was done with the assumption of transmission through AWGN Channel. Realistic LTE wireless channel will be dealt with in the next chapter.

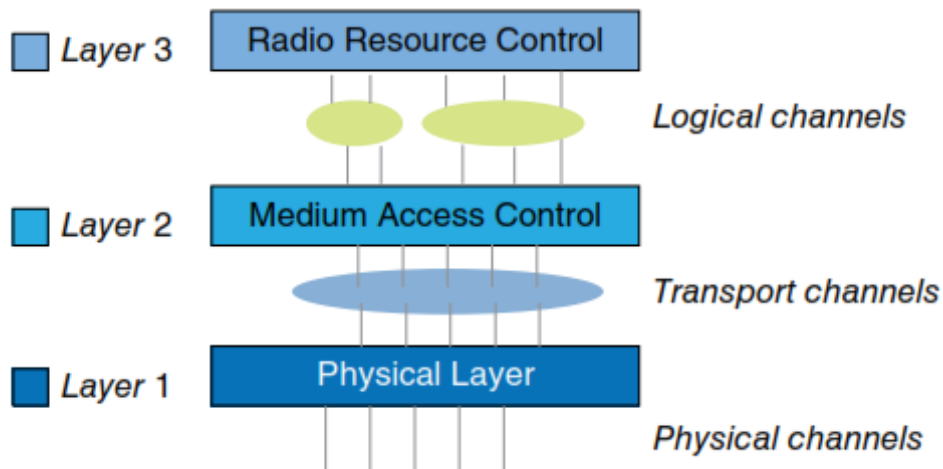


**Fig. 3.1** LTE network architecture [1]

### 3.1 LTE Physical Layer (PHY)

The LTE network architecture is illustrated in Fig. 3.1, out of which only the LTE Physical Layer was necessary for the project. LTE PHY includes the processing performed on bits of data that are handed down to the PHY, from the higher layers. It explains the mapping of physical channels to transport channels, their signal processing operations, and how data are ultimately transmitted through the antenna.

### 3.1.1 Block Diagram of LTE-PHY

Fig. 3.2 illustrates the LTE downlink PHY model, the dotted lines representing the modules used in this chapter. This can be broadly divided into two sections:

First, the data is multiplexed and encoded in a step known as Downlink Shared Channel processing (DLSCH). It involves attaching a CRC code for error detection, segmenting the data into smaller chunks known as sub-blocks, undertaking channel-coding operations based on turbo coding for the user data, carrying out a rate-matching operation that selects the number of output bits to reflect a desired coding rate, and finally reconstructing the codeblocks into codewords.

The next phase is termed Physical Downlink Shared Channel Processing (PDSCH). Here, the codewords first become subject to a scrambling operation and then undergo a modulation mapping that results in a modulated symbol stream. Precoding and layer mapping are the two MIMO operations. Precoding scales and organizes symbols allocated to each sub-stream and layer mapping selects and routes data into each substream to implement one of the nine MIMO modes specified for downlink. The final step is the multicarrier transmission, which is based on the OFDM scheme in downlink.

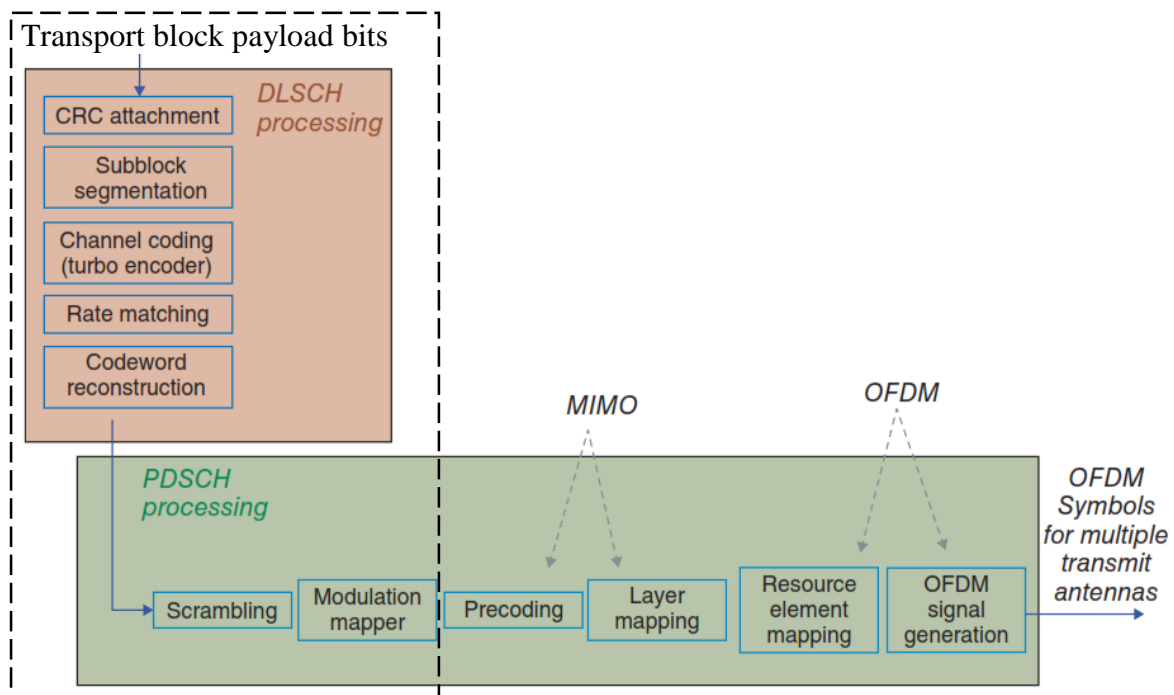
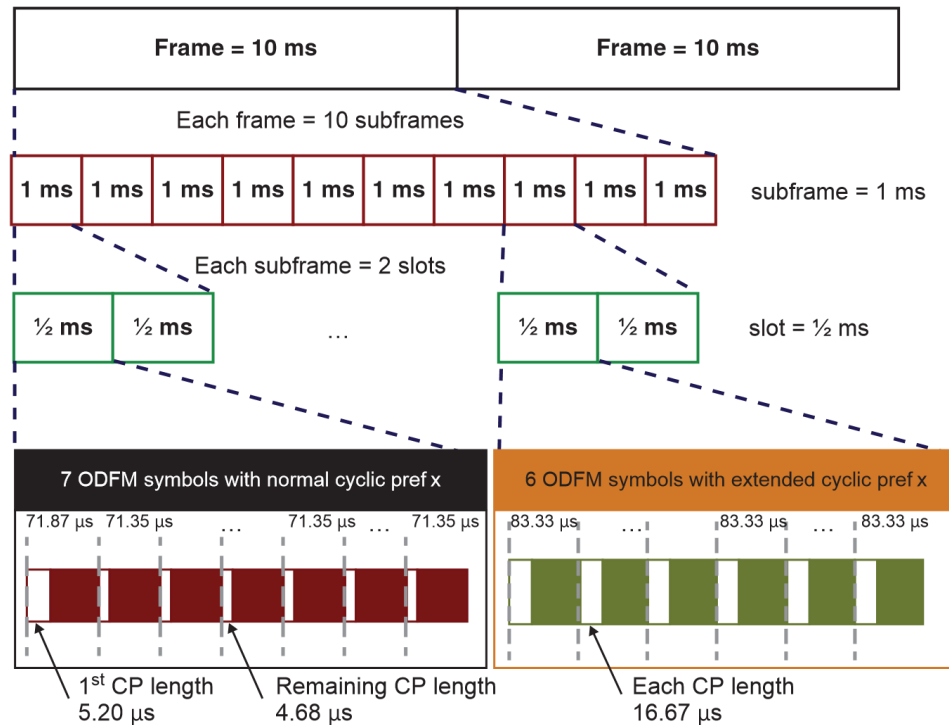


Fig. 3.2 Physical layer specifications in Downlink LTE [1]

### 3.1.2 PHY Properties

1. Frequency Bands - ITU IMT Advanced (International Telecommunications Union International Mobile Telecommunication) has stated, the paired bands used in FDD duplex mode are numbered from 1 to 25 and the unpaired bands used in TDD mode are numbered from 33 to 43. FDD is the scheme used in the project.
2. Allocation of Bandwidth - The IMT-Advanced guidelines require spectrum flexibility in the LTE standard, which is manifested by a list of spectrum allocations ranging from 1.4 to 20MHz. The frequency spectra in LTE are formed as concatenations of resource blocks consisting of 12 subcarriers. Since subcarriers are separated by 15kHz, the total bandwidth of a resource block is 180kHz. This enables transmission bandwidth configurations of from 6 to 110 resource blocks over a single frequency carrier.
3. Time Framing - In the time domain, LTE organizes the transmission as a sequence of radio frames of length 10ms. Each frame is then subdivided into 10 subframes of length 1ms. Each subframe is composed of two slots of length 0.5ms each. Finally, each slot consists of a number of OFDM symbols, either seven or six depending on whether a normal or an extended cyclic prefix is used. Fig. 3.3 shows the LTE time-domain structure.
4. Time-Frequency Representation - The most attractive feature of OFDM is that it maps explicitly to a time-frequency representation for the transmitted signal. After coding and modulation, a transformed version of the complex-valued modulated signal, the physical resource element, is mapped on to a time-frequency coordinate system, the resource grid. LTE Resource Grid, and subframe structure are shown in Fig. 4.1, 4.2 respectively. The resource grid has time on the x-axis, indicating the OFDM symbol to which it belongs and frequency on the y-axis, which signifies the OFDM subcarrier to which it belongs.

Before modulation and coding can happen, inputs from the upper layer to each block must be clearly mapped. This logical mapping is termed as PHY Processing.



**Fig. 3.3** LTE time-domain structure [1]

### 3.2 PHY Processing

Fig. 3.4 shows the mapping of the three LTE downlink channels. The operations performed by each channel is as follows:

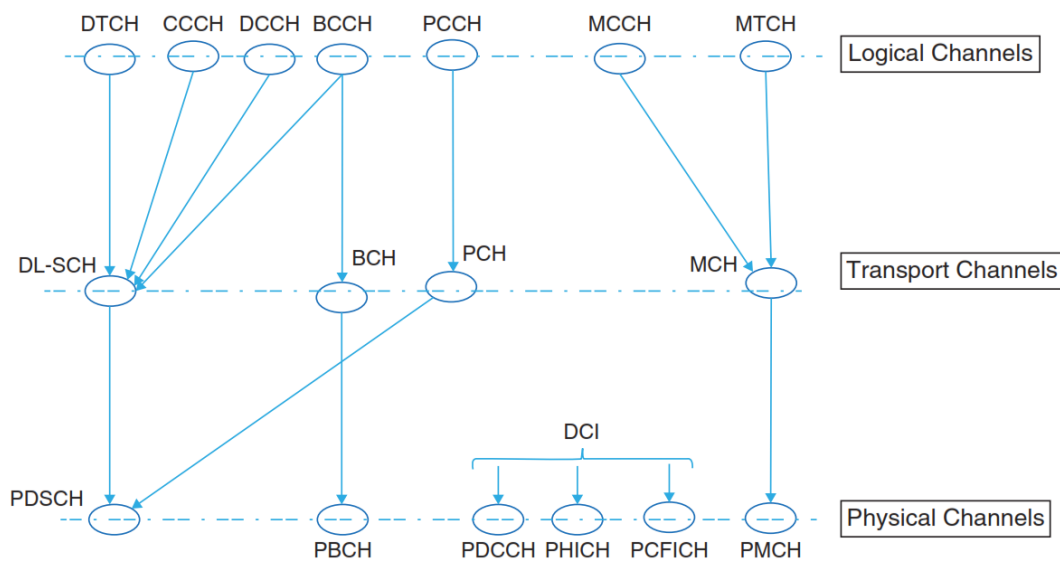


**Fig. 3.4** Mapping LTE downlink logical, transport, and physical channels

1. Logical channels represent the data transfers and connections between the radio link control (RLC) layer and the Medium Access Control (MAC) layer.
2. Transport channels connect the MAC layer to the PHY and the physical channels are processed by the transceiver at the PHY. Data transmission in downlink and uplink uses the DL-SCH (Downlink Shared Channel) and UL-SCH (Uplink Shared Channel) transport channel types respectively.
3. Physical channel contain the time-frequency resources used for sending a transport channel. Each transport channel is mapped to a physical channel. Each physical channel is specified by a set of resource elements carrying information from higher layers of the protocol stack for eventual transmission on the air interface.

### 3.3 Modulation and Coding

This chapter will first, describe channel coding, scrambling, and modulation resulting in modulated symbols. Each block will be performance measured according to elapsed time and BER vs SNR plots. A standard input-output scheme has been used for all the BER generation function, and is shown below in Table 3.1.

**Table 3.1** BER calculation functions

SL NO	FUNCTION INPUT PARAMETERS	FUNCTION OUTPUT
1	Modulation mode (QPSK, 16-QAM, 64-QAM)	BER
2	SNR $E_b/N_0$ – Given as a range in the main program	
3	Maximum acceptable errors in a transmission	Number of bits processed
4	Maximum number of bits sent in a transmission	

Typical values of acceptable errors is 200 and number of transmitted bits is 10 million, the range of SNR varying from one block to another, typically 1 to 3 dB.

### 3.3.1 Modulation Schemes

The modulation schemes used in the LTE standard include QPSK (Quadrature Phase Shift Keying), 16QAM (Quadrature Amplitude Modulation), and 64QAM. Fig. 3.5 shows the constellation diagrams of these three modulation schemes.

In the case of QPSK modulation, each modulation symbol can have one of four different values, which are mapped to four different positions in the constellation diagram. QPSK needs 2 bits to encode each of its four different modulation symbols. Similarly, 16QAM modulation involves using 16 different signalling choices and thus utilizes 4 bits of information to encode each modulation symbol, and 64QAM modulation involves 64 different possible signalling values and thus requires 6 bits to represent a single modulation symbol.

1. QPSK – It is the most often used scheme since it does not suffer from BER degradation while the bandwidth efficiency is increased. In a QPSK system, data bits are divided into groups of two bits, called dibits. There are four possible dibits, 00, 01, 10, and 11. Each of the four QPSK signals is used to represent one of them. The signal constellation in Fig. 3.5 uses the Gray coding. In QPSK, the phase of the carrier takes on one of the four values, such as  $\pi/4$ ,  $3\pi/4$ ,  $5\pi/4$  and  $7\pi/4$ . The transmitted signal can be defined as:

$$S_i(t) = \begin{cases} \sqrt{2E/T} \cos[2\pi f_c t + (2i - 1)\pi/4] & 0 \leq t \leq T \\ 0 & \text{otherwise} \end{cases} \quad (3.1)$$

Where  $i = 1, 2, 3, 4$ .  $E$  is the transmitted energy per symbol,  $T$  is the symbol duration and the carrier frequency  $f_c$ . Each possible value of the phase corresponds to a dabit.

The two orthogonal basis functions are given by:

$$\phi_1(t) = \sqrt{\frac{2}{T}} \cos(2\pi f_c t) \quad (3.2)$$

$$\phi_2(t) = \sqrt{\frac{2}{T}} \sin(2\pi f_c t) \quad (3.3)$$

There are four message points and associated signal vectors are defined by equation (3.1). A QPSK signal has a two-dimensional constellation and four message points as illustrated in Fig 3.5 A. The transmitted signal energy per symbol is twice the signal energy per bit.

$$E = 2E_b$$

The average probability of symbol error in terms of the ratio  $E_b/N_o$

$$P_e = \operatorname{erfc}(\sqrt{E_b/N_o})$$

The bit error of QPSK is given by:

$$\text{BER} = \frac{\operatorname{erfc}(\sqrt{E_b/N_o})}{2} \quad (3.4)$$

2. **QAM** - Modulation involves transmitting a sequence of waveforms  $s_i(t)$  of equal duration  $T$ , where each waveform is chosen independently from a set of  $M$ . This allows us to transmit up to  $b = \log_2 M$  bits per symbol. A common sets of such symbols are those where the real and imaginary parts of the complex baseband signal are each modulated in amplitude. This known as Quadrature Amplitude Modulation (QAM).

Some of the common forms of QAM include 16 QAM, 32 QAM, 64 QAM, 128 QAM, and 256 QAM. The number of points on the constellation, as shown in Fig. 3.5 the number of distinct states that can exist.

The various flavours of QAM may be used when data-rates beyond those offered by 8-PSK are required by a radio communications system. This is because QAM achieves a greater distance between adjacent points in the I-Q plane by distributing the points more evenly. And in this way the points on the constellation are more distinct and data errors are reduced. While it is possible to transmit more bits per symbol, if the energy of the constellation is to remain the same, the points on the constellation must be closer together and the transmission becomes more susceptible to noise. This results in a higher bit error rate than for the lower order QAM variants. In this way there is a balance between obtaining the higher data rates and maintaining an acceptable bit error rate for any radio communications system.

M-ary QAM is a two dimensional generalization of M-ary PAM. Thus, its formulation involves two orthogonal passband basis functions:

$$\phi_1(t) = \sqrt{\frac{2}{T}} \cos(2\pi f_c t) \quad (3.5)$$

$$\phi_2(t) = \sqrt{\frac{2}{T}} \sin(2\pi f_c t) \quad (3.6)$$

The signal constellation for 16 QAM and 64 QAM is shown in figures 3.5 B and 3.5 C. The signal constellation diagram consists of both in-phase and quadrature components. If  $E_b$  is the energy of the signal with lowest amplitude, the generalized equation for probability of error of a M-ary QAM system is given by:

$$P_e = 2\left(1 - \frac{1}{\sqrt{M}}\right) \operatorname{erfc}\left(\sqrt{\frac{E_b}{N_0}}\right) \quad (3.7)$$

M=16,

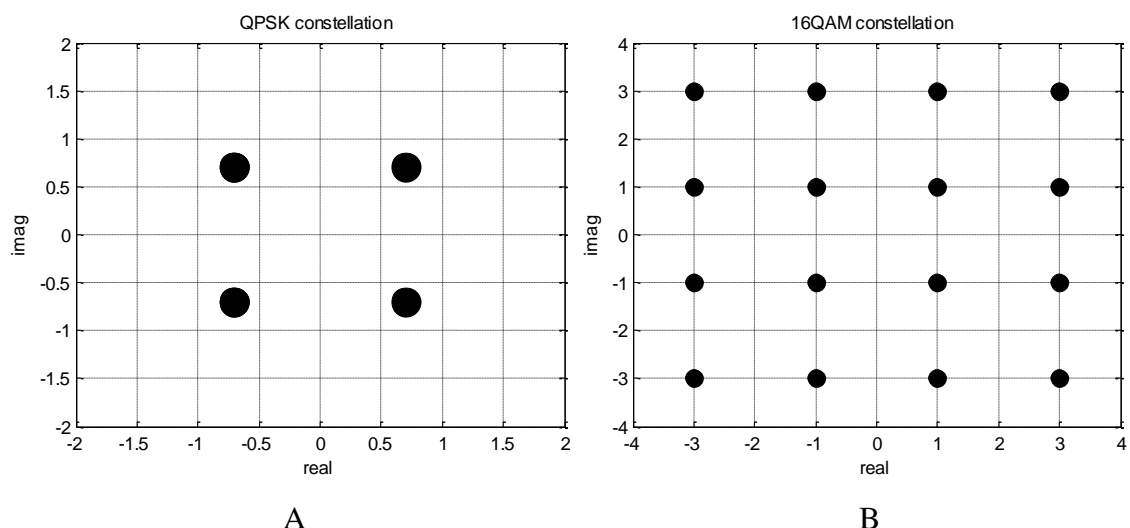
$$P_e = 1.5 \operatorname{erfc}(\sqrt{E_b/N_o})$$

M=64,

$$P_e = 1.75 \operatorname{erfc}(\sqrt{E_b/N_0})$$

**Table 3.2** Modulator function

<b>SL NO</b>	<b>FUNCTION INPUT PARAMETERS</b>	<b>FUNCTION OUTPUT</b>	<b>SYSTEM OBJECTS USED</b>
1	Input bit stream	Modulated symbols	QPSK – comm.PSKModulator
2	Modulation mode (QPSK, 16-QAM, 64-QAM)		16, 64 QAM – comm. RectangularQAMModulator



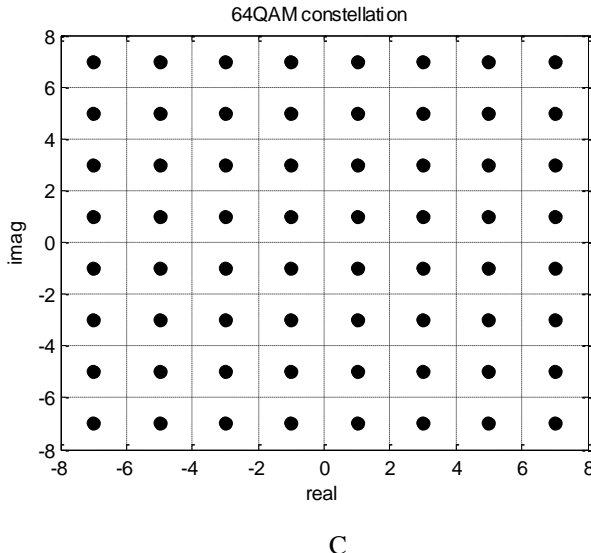


**Fig. 3.5** Constellation diagram of A – QPSK, B – 16-QAM, C – 64-QAM

From the above discussion, it is clear that the distance between the message points of the M-ary PSK goes on decreasing as M increases leading to errors. Also, QAM outperforms QPSK in noise performance.

The availability of multiple modulation schemes is instrumental in implementing adaptive modulation based on channel conditions, and is one of the biggest improvements LTE provides.

When the radio link is relatively clean – that is, the Signal-to-Noise Ratio (SNR) is relatively high – modulation schemes of denser constellations such as 64QAM can be used. In such a case, sending a single symbol results in the transmission of 6 bits and therefore can increase our throughput. However, as the channel becomes noisier, using modulation schemes with more intersymbol separation such as QPSK was found as the right choice. This in turn will reduce the number of bits per sample and reduce the throughput.

### 3.3.2 Demodulation

All the receiver specifications presented in this chapter can be considered ‘inverse’ of operations specified in the transmitter. Demodulation is primarily based on either hard-decision, where the input symbols are mapped to estimated bits, or soft-decision decoding, input symbols being a vector of log-likelihood ratios (LLRs). Soft-decision decoding will be incorporated in all further discussions.

Table 3.3 describes the Demodulator function parameters. From Fig. 3.6, it can be inferred that BER performance of QPSK is better than the other two modulation schemes when there is a high signal-to-noise ratio. Whereas, the performance of 16-QAM and 64-QAM deteriorates with increase in SNR. QAM schemes perform better even at low SNR values.

**Table 3.3** Demodulator function

SL NO	FUNCTION INPUT PARAMETERS	FUNCTION OUTPUT	SYSTEM OBJECTS USED
1	Received bit stream	Demodulated symbols	QPSK – comm.PSKDemodulator
2	Demodulation mode (QPSK, 16-QAM, 64-QAM)		16, 64 QAM – comm. RectangularQAMDemodulator

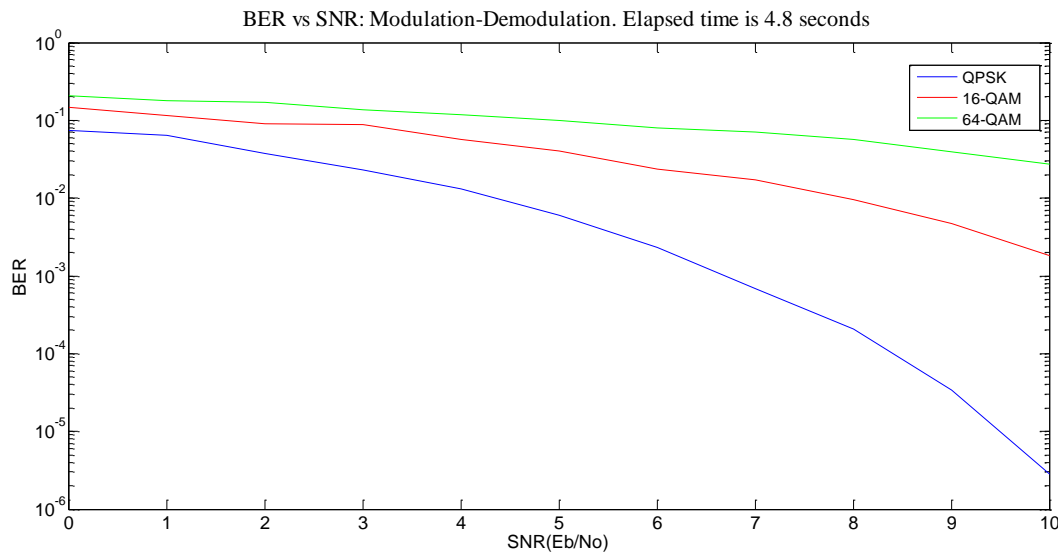


**Fig. 3.6** BER vs SNR plot – Modulation-Demodulation

### 3.3.3 Scrambling

A bit-level scrambling sequence is used on the codeword bits formed in channel coding. Different scrambling sequences are used in neighbouring cells to ensure that the minimised interference. Based on the PHY cell identity, the sequence generators in the cell are initialized.

Scrambling is composed of two stages: pseudo-random sequence generation and bit-level multiplication. In the first stage, the sequence is generated by a Gold sequence of length 31. The output is an exclusive-or operation applied to polynomials specifying this pair of sequences. The polynomials specifying this pair of sequences are as follows:

$$p_1(x) = x^{31} + x^3 + 1$$

$$p_2(x) = x^{31} + x^3 + x^2 + x + 1$$

Since a scrambling operation helps in inter-cell interference mitigation, the plot obtained earlier in Figure 3.6 are smoothed.

**Table 3.4** Scrambler function

SL NO	FUNCTION INPUT PARAMETERS	FUNCTION OUTPUT	SYSTEM OBJECTS USED
1	Input bit stream	Scrambled sequence	comm.GoldSequence
2	Subframe index of the current frame		comm.IntegerToBit

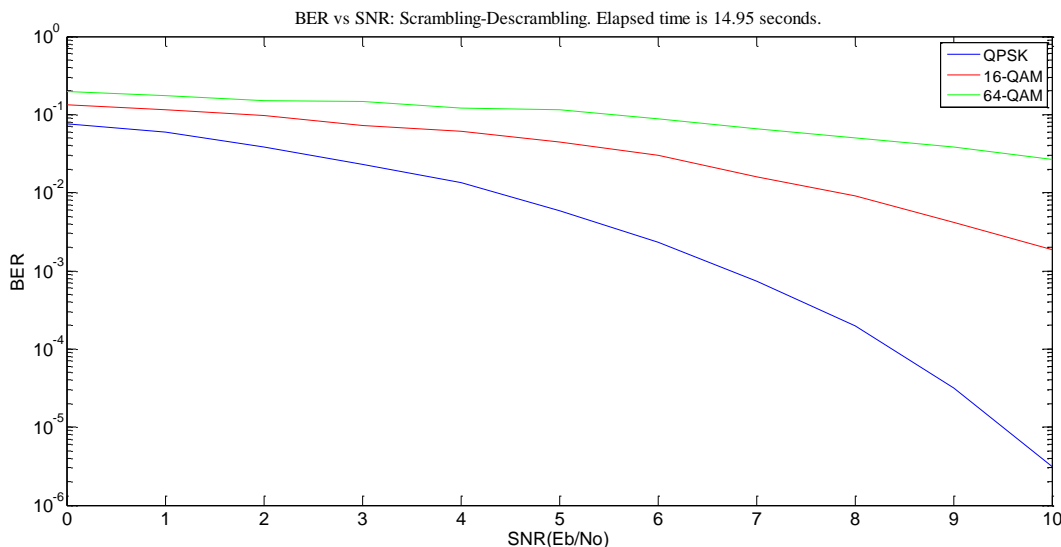


**Fig. 3.7** BER vs SNR plot – Scrambling-Decrambling

Descrambling is the reverse of this operation, involving exclusive-or operation and PN-sequence extraction respectively. Owing to the similarity of receiver blocks, the receiver table of Turbo decoder, Rate de-matcher will not be dealt with.

**Table 3.5** Descrambler function

SL NO	FUNCTION INPUT PARAMETERS	FUNCTION OUTPUT	SYSTEM OBJECTS USED
1	Received bit stream	Descrambled sequence	comm.GoldSequence
2	Subframe index of the current frame		comm.IntegerToBit

### 3.3.4 Turbo Coding

Turbo coders belong to parallel concatenated convolutional category of coding [2]. Turbo codes are formed by concatenating two conventional encoders in parallel, each of which is separated by an interleaver.

LTE uses turbo coding with a base rate of 1/3 for its channel-coding scheme. It has a parallel concatenation of two 8-state encoders separated by an interleaver. The output is made of three streams. The first stream is referred to as Systematic bits, whereas the second and third streams: outputs of the two encoders – are referred to as Parity 1 and Parity 2, respectively. Each encoder is independently terminated by tail bits. So for an input block size of K bits, the output is made of three streams of length K+ 4 bits. The relationship between the output  $p(i)$  and the input index  $i$  is related by the quadratic polynomial expression:

$$p(i) = (f_1 \cdot i + f_2 \cdot i^2) \bmod(k)$$

where  $K$  - size of the input block

$f_1$  and  $f_2$  - constants depending on  $K$ .

For LTE, the input block size  $K$  can have 188 different values, the smallest block size being 40, up to 6143.

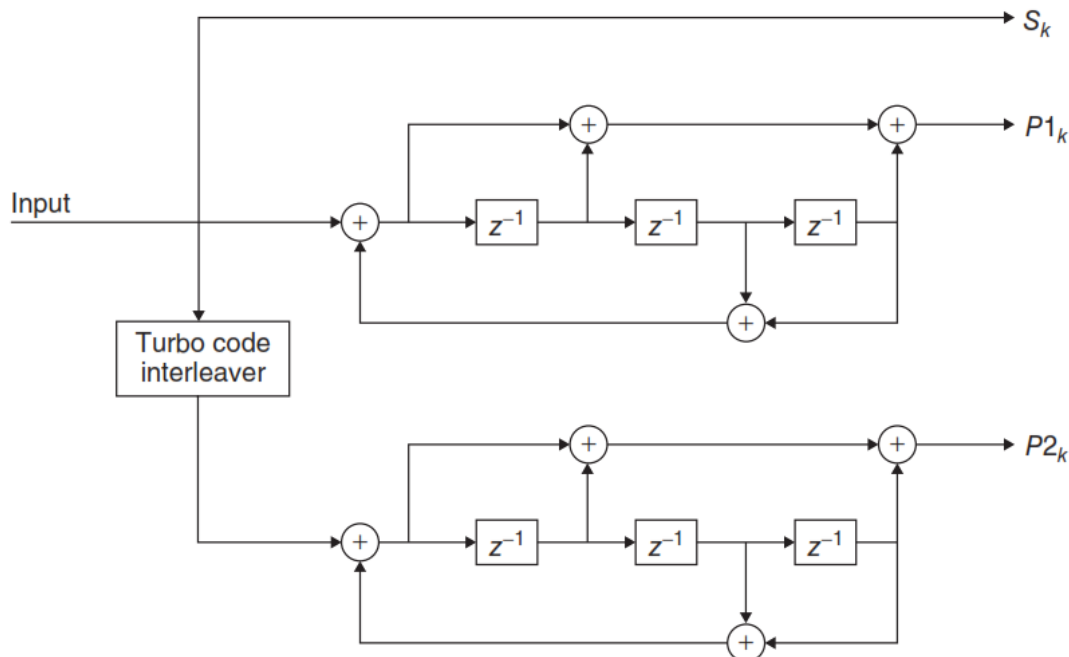


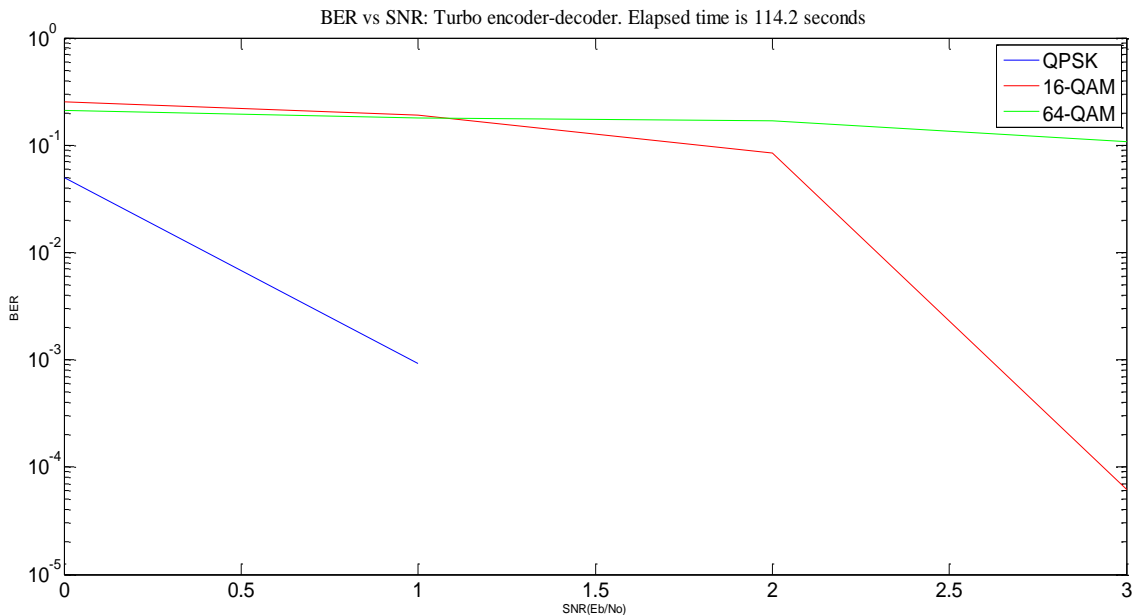
**Fig. 3.8** Block diagram of a turbo encoder

**Table 3.6** Turbo-Encoder function

SL NO	FUNCTION INPUT PARAMETERS	FUNCTION OUTPUT	SYSTEM OBJECTS USED
1	Input bit stream	Turbo-Encoded bits	comm.TurboEncoder
2	Interleaving indices (generated by a function)		Ploy2trellis

At the UE, turbo decoder inverts the operations performed at the encoder. Two A-posteriori Probability (APP) decoders and two interleavers are used in a feedback loop. APP decoder uses the same trellis structure as in encoder, as is the same interleaver. The decoder's complexity directly relates to the number of iterations. The turbo decoder input needs to be expressed in LLRs, so soft-decision demodulation is used. The Decoder function table is the same as that of encoder.

For three iterations, an approximate of 197 seconds was required, with 1.44 million bits processed, out of which 203 bits had errors.


**Fig. 3.9** BER vs SNR plot –Turbo Encoder-Decoder

### 3.3.5 Early termination mechanism

The turbo decoder's accuracy and performance depends on number of iterations, but takes a lot of time for execution, which real-time LTE systems cannot afford.

LTE provides a solution to this tradeoff by proposing early termination mechanism, which is integrated with the turbo encoder. This is achieved by appending a CRC checking syndrome as encoder's input, which helps detect the presence of bit errors at the end of every iteration. There is now an option of stopping the decoding early at an iteration, if the CRC check does not indicate any error. Table 3.7 describes the Early termination function, whose output is shown in Fig. 3.10. There is a huge reduction in the elapsed time as compared to standard Turbo coding.

**Table 3.7** Early termination function

SL NO	FUNCTION INPUT PARAMETERS	FUNCTION OUTPUT	SYSTEM OBJECTS USED
1	Input bit stream	Turbo-Encoded and Decoded bits	comm.CRCGenerator
2	Interleaving indices (generated by a function)		comm.CRCDetector

```
>> EbNo=1; maxNumErrs=1e7; maxNumBits=1e7;
tic; [a,b]=Turbo(EbNo,maxNumErrs, maxNumBits); toc;
tic; [a,b]=Early_Termination(EbNo,maxNumErrs, maxNumBits); toc;
Elapsed time is 197.800292 seconds.
Elapsed time is 116.198952 seconds.
```

**Fig. 3.10** Comparison of Turbo Coding, without and with Early Termination

### 3.3.6 Algorithm for Rate Matching

A turbo coding operation with a coding rate of 1/3 has been considered so far. Implementation of adaptive coding involves rate matching. It helps augment the throughput based in the channel conditions. In the case of low-distortion channels, the data with coding rates near unity can be coded, which reduces the number of bits transmitted for forward error coding. In degraded channels, the number of error-correction bits can be increased by using smaller coding rates.

In channel coding with rate matching, a constant 1/3-rate turbo coder is used along with rate matching to arrive at any desired rate. If a rate lower than 1/3 is requested, the turbo coder output bits are repeated. For rates higher than 1/3, some of the turbo coder output bits are punctured or removed. The puncturing of the code is based on an

interleaving method. Rate matching is composed of: interleaving of subblock, Parity-bit interlacing, bit selection and transmission based on rate.

**Table 3.8** Rate Matching function

SL NO	FUNCTION INPUT PARAMETERS	FUNCTION OUTPUT
1	Output from 1/3 Turbo Encoder	Rate-matched output to Turbo-decoder
2	Block size	

After early termination and rate matching, an approximate of 66 seconds was taken to process 5 million bits in three iterations, with 24 errors. This is a drastic improvement as compared to the previous result. Fig. 3.11 compares BER vs SNR for 1/2 and 1/3 rate coding. Thus, each block iteratively improves the performance of LTE coding scheme.

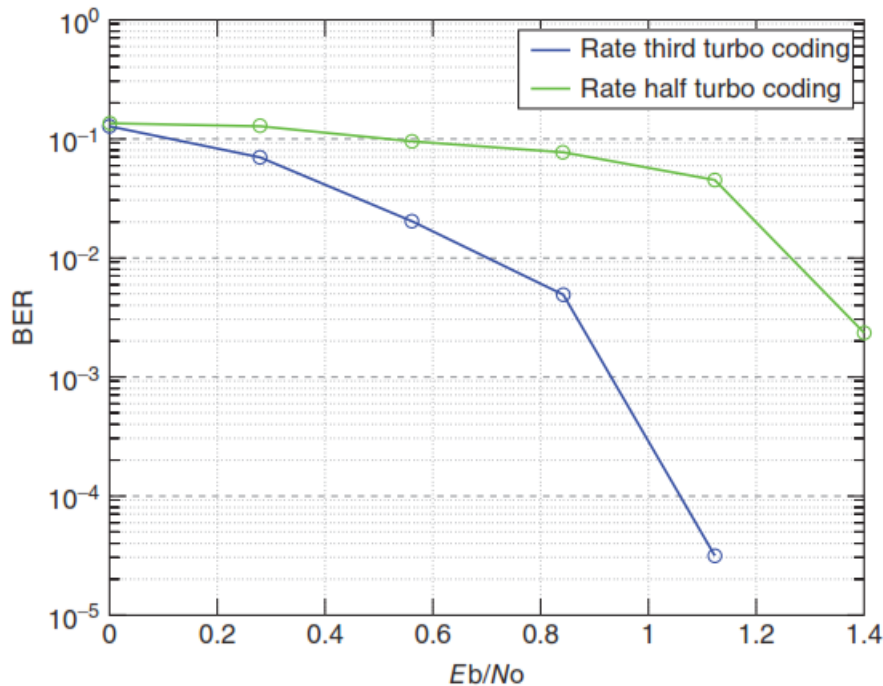


**Fig. 3.11** BER vs SNR plot for 1/3 and 1/2 rate

### 3.3.7 Channel Processing

Fig. 1.4 illustrates channel processing, which represents the overall LTE PHY Downlink block. An AWGN channel is included between the channel Encoder and Decoder sections.

Channel Encoding - Five functional components characterize transport block processing:

- Transport-block CRC attachment
- Codeblock segmentation and codeblock CRC attachment
- Turbo coding based on a 1/3 rate
- Rate matching to handle any requested coding rates
- Codeblock concatenation

Channel Decoding - The sequence of operations performed in channel decoding can be regarded as the inverse of those performed in channel coding, as follows:

- Iteration over each codeblock
- Rate dematching (from target rate to 1/3 rate) composed of:
  - Bit selection and insertion
  - Parity-bit deinterlacing
  - Subblock deinterleaving
  - Recovery of Systematic and Parity bits for turbo decoding
- Codeblock 1/3-rate turbo decoding with early termination based on CRC.

### 3.4 Summary

An AWGN channel based transceiver, as shown in Fig. 1.4, has been successfully simulated for the LTE PHY modeling in MATLAB. By running the overall function with a series of  $E_b/N_0$  values and changing the *ModulationMode* parameter, the relationship between modulation order and robustness to channel noise was observed.

All the blocks were tested through a random input generated by MATLAB and passing it throughout the chain of both transmitter, receiver blocks. If the input was same as the output, then it was confirmed that the blocks are functioning as prescribed. The entire set of blocks used in this chapter will be represented by a single function in further chapters. This will simplify debugging operations and help in re-usage of blocks. In the next Chapter, a realistic LTE-specific channel will be dealt with.

## *Chapter 4*

### ***Pilot-based OFDM Channel Estimation***

## CHAPTER 4

### PILOT-BASED OFDM CHANNEL ESTIMATION

In the previous chapter, a simplistic channel model, the Additive White Gaussian Noise (AWGN) was used to evaluate the performance of the modulation and coding schemes of the LTE standard. However, in order to understand OFDM, which is the fundamental air interface in the standard, modelling of more sophisticated channel models than AWGN have to be considered. These channel models must take into account dynamic channel responses and fading conditions. Section 4.1 illustrates realistic channel models that take these conditions into account are considered.

Represented by dotted lines in Fig. 4.1, Section 4.2 explains the frame structure of OFDM and its configuration as per LTE standard. Section 4.3 talks about Pilot signal generation. Time–frequency mapping of the OFDM signal and various resource element granularities which are used to adaptively exploit the channel bandwidth is looked at in Section 4.4. Section 4.5 details the OFDM signal generation. Section 4.6 estimates the channel impulse response, whereas Section 4.7 Frequency-domain equalization of the OFDM signal at the receiver utilising Zero Forcing (ZF) and Minimum Mean Squared Error (MMSE) equalizers. A summary of the entire procedure is provided in Section 4.8.

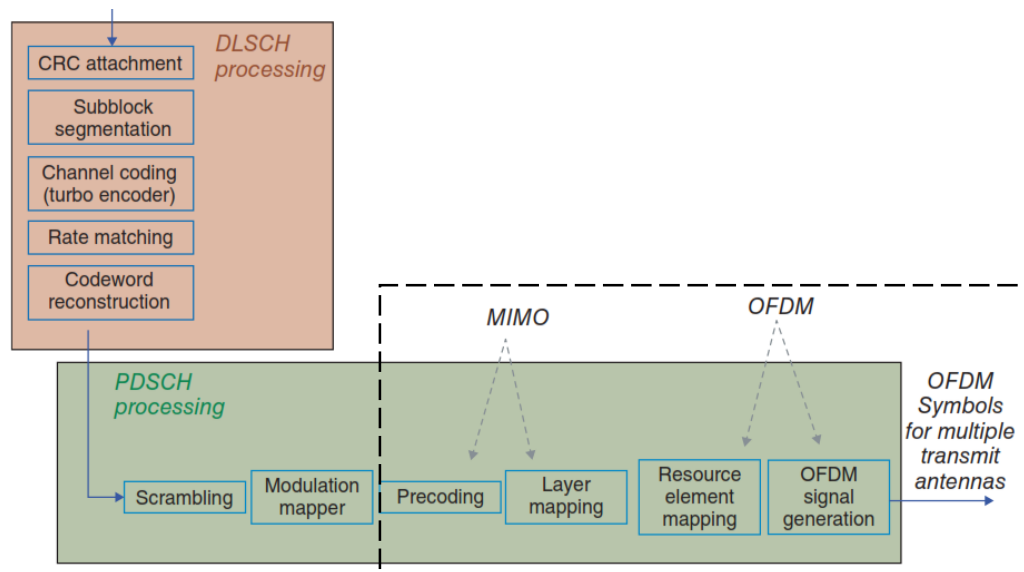


**Fig. 4.1** Physical layer specifications in Downlink LTE [1]

## 4.1 Realistic Channels

The paths of propagation between transmitters and receivers can comprise of either a direct path between the transmitter and the receiver or paths that are formed as a result of various propagation scenarios such as reflection, diffraction and scattering among others. The availability of these different propagation paths characterizes wireless channels. The signals, on being transmitted through these different paths, will have different signal power profiles, time delay and phase, while being received simultaneously at the receiver. As these received signals are correlated in time, an AWGN channel alone is insufficient for the modelling of most wireless communication systems.

Channel propagation results in reduced power of received signals compared to transmitted signals and these power reductions are of two types:

1. Large-scale fading or signal attenuation - This includes Path loss and shadowing effects which are taken into account in design and cellular topography [34].
2. Fading or Small-scale fading - This includes multipath fading and time dispersion due to mobility. These are of short duration and must be taken into account in the design.

Therefore, proper modelling of the wireless channel must include techniques that deal with these types of channel impairments [34], the description of which is as follows:

### 4.1.1 Multipath Fading

In wireless communication systems involving multipath propagation, the signals are received at the mobile terminal either via a direct path between the transmitter and the receiver or being reflected off buildings or other reflectors. As a result, the received signal is a convolution of the input signals and the impulse response of the channel. Therefore, the power profile comprises of two vectors, a vector of average delays and a vector of average power parameters.

Multipath fading can either be flat or frequency selective fading. In the frequency domain, as different response patterns are present at different frequencies, frequency selective fading is the chosen one.

#### 4.1.2 Doppler Effects

In LTE, the predominant channel degradation occurs due to short-term fading. Fast and slow fading channels mobile terminal movement in terms of Doppler frequency shifts. This leads to variations in the impulse response profiles [35].

#### 4.1.3 MATLAB Tools for realistic channels

The Communications System Toolbox is used to study the effect of channel responses under various channel models:

1. Rician and Rayleigh channel System objects to model a single propagation path
2. *comm.MIMOChannel* System object represent the effects of multi-propagation paths and multiple antennas

To model the dynamics of the fading channels, these components use Doppler shift and delay profiles as parameters and obtain four different combinations.

The system model is obtained by adding flat or frequency selective fading for coding, modulation and scrambling. By considering reference signal generation, resource grid specification and OFDM transmission, a test-bench for the first mode of downlink transmission is implemented.

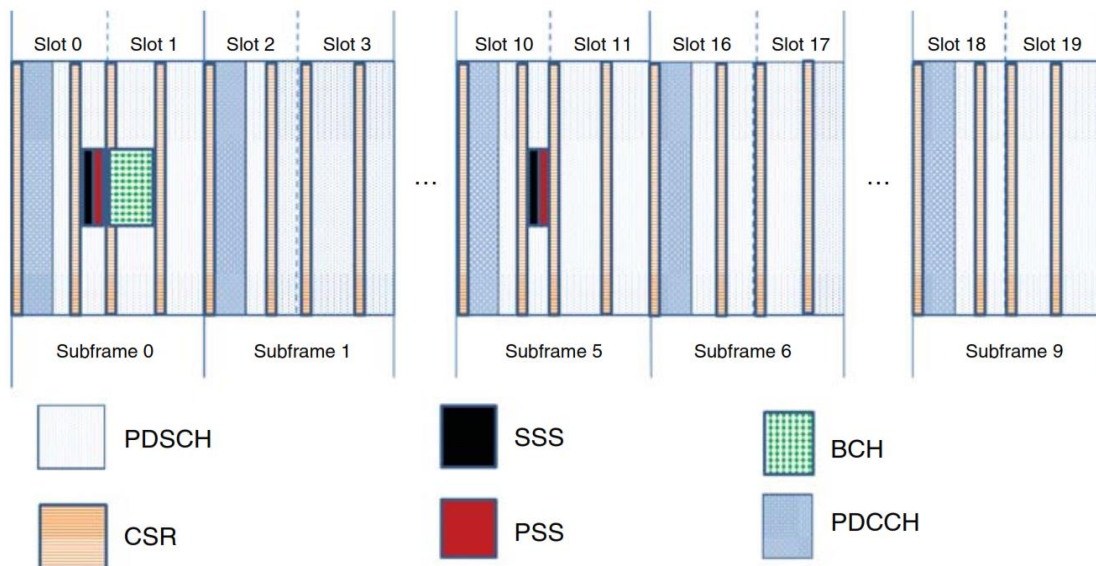


**Fig. 4.2** LTE resource grid content [1]

## 4.2 Configuring the LTE Resource Grid

The LTE resource grid comprises of time-frequency representation of data. The placement of the data in the resource grid reveals the design parameters of the LTE physical model. For instance, the accuracy of the channel response is determined by the placement and resolution of pilot signals (CSR). The resource grid is organised as a 2 dimensional resource grid comprising of subcarriers along the frequency dimensions (y-axis) and OFDM symbols along the time dimension (x-axis).

Fig. 4.1 illustrates the placement of different modulated data based on the signal types, within the resource grid. All subframes within a frame contain three types of information: user data (PDSCH), pilot CSRs, and downlink control data (PDCCH). The PSS and SSS are only available in subframes 0 and 5, SSS at fifth symbol and PSS at sixth symbol and specific subcarrier indices (72 subcarriers around the center of the resource grid). The PBCH is located only within subframe 0 at specific OFDM symbol indices. Fig. 4.2 illustrates the structure of the LTE Resource Grid, whereas Fig. 4.4 shows the configuration parameters, whose output is displayed in Fig. 4.5, 4.6 with Modulation mode, Bandwidth variations.

### 4.2.1 CSR Symbols – Pilot Signals

In each subframe, CSRs are placed in a specific time and frequency separation per resource block. In the single-antenna configuration, LTE specifies two CSR symbols per resource block in each of the four OFDM symbols {0, 5, 7, 12} in any subframe, as per Fig. 4.3. In OFDM symbols 0 and 7, the starting indices are the first subcarrier, whereas in symbols 5 and 12 the starting index is the fourth subcarrier. There are a total of  $N_{CSR} = 8N_{rb}$  CSR symbols available in the resource grid. In all the functions used,  $N_{rb}$  is taken as 6, equivalent to a Bandwidth of 1.4MHz.

**Table 4.1** Resource Grid Configuration

SL NO	FUNCTION INPUT PARAMETERS	FUNCTION OUTPUT
1	Channel Bandwidth	Configured Grid Structure
2	OFDM symbols per subframe	
3	Modulation Mode	

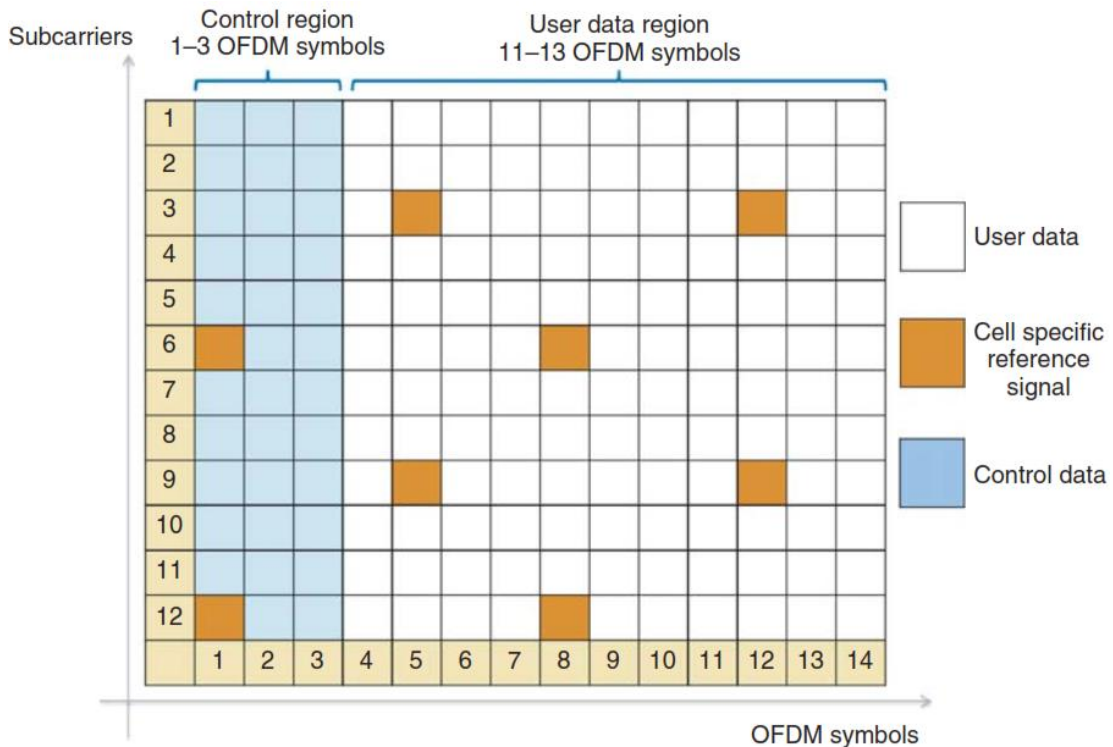


Fig. 4.3 Signal content of LTE downlink subframe [1]

```

switch chanBW
case 1 % 1.4 MHz
    BW = 1.4e6; N = 128; cpLen0 = 10; cpLenR = 9;
    Nrb = 6; chanSRate = 1.92e6;
case 2 % 3 MHz
    BW = 3e6; N = 256; cpLen0 = 20; cpLenR = 18;
    Nrb = 15; chanSRate = 3.84e6;
case 3 % 5 MHz
    BW = 5e6; N = 512; cpLen0 = 40; cpLenR = 36;
    Nrb = 25; chanSRate = 7.68e6;
case 4 % 10 MHz
    BW = 10e6; N = 1024; cpLen0 = 80; cpLenR = 72;
    Nrb = 50; chanSRate = 15.36e6;
case 5 % 15 MHz
    BW = 15e6; N = 1536; cpLen0 = 120; cpLenR = 108;
    Nrb = 75; chanSRate = 23.04e6;
case 6 % 20 MHz
    BW = 20e6; N = 2048; cpLen0 = 160; cpLenR = 144;
    Nrb = 100; chanSRate = 30.72e6;
end

```

Fig. 4.4 LTE resource grid configuration: Parameter variation for different Bandwidths

### 4.3 Pilot Signal Generation

LTE uses Gold sequences in order to ensure that the same reference sequence is generated by both the transmitter and the receiver. These Gold sequences are generated by using parameters that are available to both the transmitter and the receiver. These parameters include cell identity number, subframe, and slot and OFDM symbol index containing the CSR in the slot. Based on the Gold sequence available at all the antenna ports, the function in Table 4.2 takes 2 input arguments and generates a matrix of CSR signals for every transmit antenna, shown in Fig. 4.7.

**Table 4.2** Pilot Signal Generation

SL NO	FUNCTION INPUT PARAMETERS	FUNCTION OUTPUT
1	Subframe Index	Matrix with CSR signals in rows for every transmit antenna in column
2	Number of Transmit Antennas	

```
>> prmsPDSCH(1, 7, 1)

ans =

    BW: 1400000
    N: 128
    cpLen0: 10
    cpLenR: 9
    Nrb: 6
    chanSRate: 1920000
    contReg: 7
    numTx: 1
    numRx: 1
    numLayers: 1
    numCodeWords: 1
    deltaF: 15000
    Nrb_sc: 12
    Ndl_symb: 7
    numResources: 1008
    numCSRResources: 48
    numContRE: 492
    numBCHRE: 276
    numSSSRE: 72
    numPSSRE: 72
    numDataRE: [3x1 double]
    numDataResources: 960
    Qm: 2
    numLayPerCW: 1
    numDataBits: 1920
    numPDSCHBits: [3x1 double]
    maxG: 936
```

```
>> prmsPDSCH(1, 7, 2)

ans =

    BW: 1400000
    N: 128
    cpLen0: 10
    cpLenR: 9
    Nrb: 6
    chanSRate: 1920000
    contReg: 7
    numTx: 1
    numRx: 1
    numLayers: 1
    numCodeWords: 1
    deltaF: 15000
    Nrb_sc: 12
    Ndl_symb: 7
    numResources: 1008
    numCSRResources: 48
    numContRE: 492
    numBCHRE: 276
    numSSSRE: 72
    numPSSRE: 72
    numDataRE: [3x1 double]
    numDataResources: 960
    Qm: 4
    numLayPerCW: 1
    numDataBits: 3840
    numPDSCHBits: [3x1 double]
    maxG: 1872
```

**Fig. 4.5** LTE resource grid configuration: fixed BW, Varying Modulation Scheme (QPSK, 16-QAM)

```
>> prmsPDSCH(1,7,1)

ans =

    BW: 1400000
    N: 128
    cpLen0: 10
    cpLenR: 9
    Nrb: 6
    chanSRate: 1920000
    contReg: 7
    numTx: 1
    numRx: 1
    numLayers: 1
    numCodeWords: 1
    deltaF: 15000
    Nrb_sc: 12
    Ndl_symb: 7
    numResources: 1008
    numCSRResources: 48
    numContRE: 492
    numBCHRE: 276
    numSSSRE: 72
    numPSSRE: 72
    numDataRE: [3x1 double]
    numDataResources: 960
    Qm: 2
    numLayPerCW: 1
    numDataBits: 1920
    numPDSCHBits: [3x1 double]
    maxG: 936

>> prmsPDSCH(2,7,1)

ans =

    BW: 3000000
    N: 256
    cpLen0: 20
    cpLenR: 18
    Nrb: 15
    chanSRate: 3840000
    contReg: 7
    numTx: 1
    numRx: 1
    numLayers: 1
    numCodeWords: 1
    deltaF: 15000
    Nrb_sc: 12
    Ndl_symb: 7
    numResources: 2520
    numCSRResources: 120
    numContRE: 1230
    numBCHRE: 276
    numSSSRE: 72
    numPSSRE: 72
    numDataRE: [3x1 double]
    numDataResources: 2400
    Qm: 2
    numLayPerCW: 1
    numDataBits: 4800
    numPDSCHBits: [3x1 double]
    maxG: 2340
```

**Fig. 4.6** LTE resource grid configuration: Varying BW (1.4, 3, 5, 10 MHz) Fixed Modulation Scheme

Appendix A provides details on Resource Element Mapping scheme, as defined and specified by LTE Release 8 specifications.

**Table 4.3** Resource Element Mapping

SL NO	FUNCTION INPUT PARAMETERS	FUNCTION OUTPUT
1	User Data	Resource Grid Matrix with rows equal to subcarriers and columns equal to symbols per subframe
2	CSR signal	
3	Subframe Index	
4	PDSCH Parameters	

**Fig. 4.7** Pilot Signal Generation

#### 4.4 Resource Element Mapping

The Resource grid matrix is created and various information types are placed within the grid, which is termed mapping. The input to the mapping function, shown in Table 4.3, is the user data, subframe index, CSR signal, parameters of the PDSCH and additional inputs depending on the availability of BCH, SSS, PSS, and DCI. The output is the 2D resource grid matrix, with number of rows equal to the number of subcarriers and number of columns, totalling 14 (two slots, each containing seven OFDM symbols).

## 4.5 OFDM Signal Generation

OFDM signal generation processes the OFDM symbols one by one and performs IFFT operation. Following this, CP generates the OFDM modulated signal.

From Table 4.4, the OFDM Generation function takes the resource grid and the structure containing the parameters of the PDSCH as input and shows the way columns of data are packed into the FFT buffer. The CP prefixes N last samples of the IFFT output to the buffer. This difference of values of N and CP for the first and remaining OFDM symbols is considered in the for loop for computing the output signal by serializing and affixing the length of OFDM modulated signal to the output vector per subframe [36]. The output is a 2D matrix of output per subframe and the number of antenna ports.

**Table 4.4** OFDM Signal Generation

SL NO	FUNCTION INPUT PARAMETERS	FUNCTION OUTPUT
1	Resource Grid Content	Matrix of output per subframe and number of antenna ports
2	PDSCH Structure	

### 4.5.1 Channel Modeling

As Table 4.5 illustrates, the inputs to this function takes are generated OFDM signal, the structures which have parameters of the PDSCH and parameters of the channel model. A frequency-flat or frequency-selective channel is applied as input based on the input parameters. The signal at the receiver is the output of the channel model. The second output, depending on the fading, is a matrix of channel-path gains. An ideal channel response can now be estimated.

**Table 4.5** Channel Modelling

SL NO	FUNCTION INPUT PARAMETERS	FUNCTION OUTPUT
1	Resource Grid Content	
2	PDSCH Structure	
3	Channel Model Structure	Signal arrived at receiver

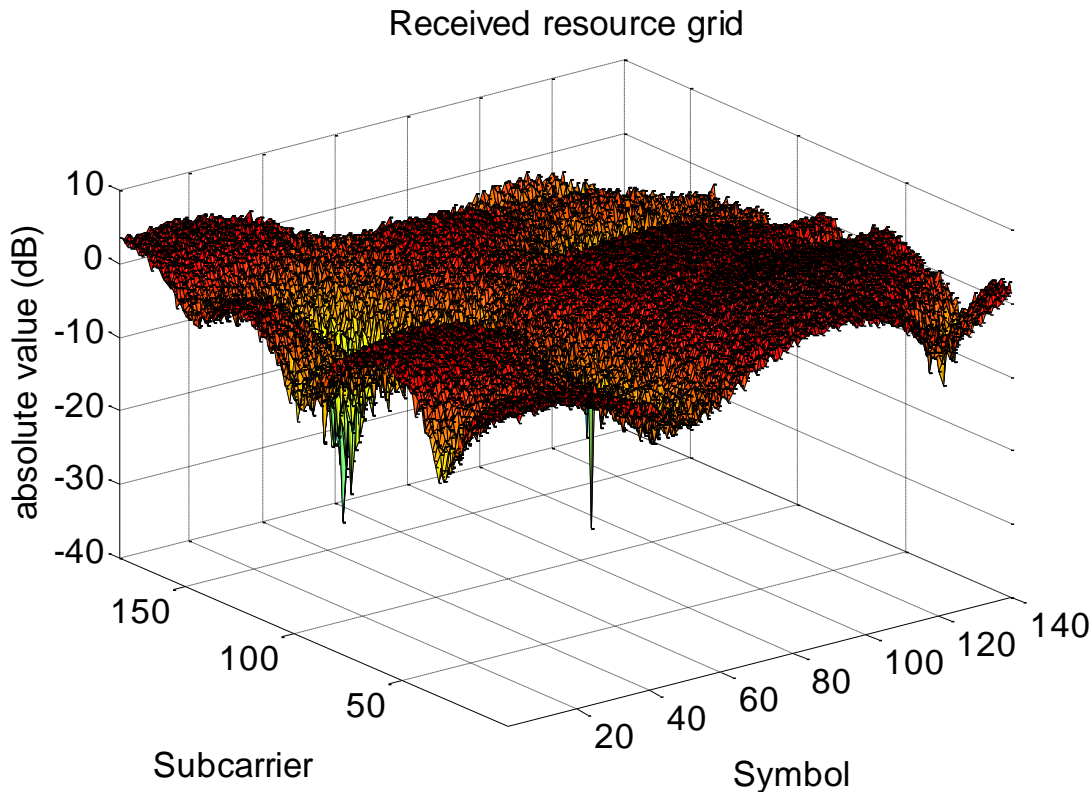


**Fig. 4.8** Received Resource Grid

#### 4.6 Inverse Operations at Receiver end

Inverse operations are performed at the OFDM receiver. The CP is removed and the received data and the reference signals are recovered by performing FFT operation. FFT lengths can be different, according to BW. The received modulated symbols are arranged into the resource grid in the same order as in the transmitter. The MATLAB function shows the series of operations performed at the OFDM receiver. The receiver input signal and the structure of the parameters of the PDSCH are the inputs in Table 4.6. OFDM receiver is verified to have successfully recovered the output resource grid, as plotted in Fig. 4.8.

**Table 4.6** OFDM Signal Reception

SL NO	FUNCTION INPUT PARAMETERS	FUNCTION OUTPUT
1	Resource Grid Content	Recovered Resource Grid Matrix with rows equal to subcarriers
2	PDSCH Structure	

## 4.7 Channel Estimation

By inspecting CSR symbols, also known as pilots, placed at regular intervals within the OFDM time–frequency grid, LTE Channel Estimation is performed. Using these reference symbols, the receiver can gauge the channel response at the subcarriers where the reference symbols were transmitted. The reference symbols should be sufficiently placed in the grid so as to estimate the channel response efficiently.

The PDSCH parameter, the receiver Resource Grid, the CSR, and bandwidth expansion mode are the inputs to the estimation function in Table 4.7. The received version of the resource grid is reshaped and aligned with the corresponding pilot elements in the CSR. An estimate of the channel-response can be computed, dividing the received pilots by the transmitted pilots.

A full bandwidth expansion is performed after channel-response matrix estimation over the resource elements aligned with CSR signals. Interpolation is performed over the entire resource grid to estimate the channel response based on reference signals in the resource grid at each subcarrier and symbol in a subframe.

**Table 4.7** Channel Estimation Function

SL NO	FUNCTION INPUT PARAMETERS	FUNCTION OUTPUT
1	Received Resource Grid	Channel Impulse Response Estimate
2	CSR signal	
3	Demodulation Mode	
4	PDSCH Parameters	

### 4.7.1 Interpolation

Interpolation algorithms typically involve interpolation between subcarriers in the frequency domain in OFDM symbols that contain reference signals. After having computed the channel response over all subcarriers, we can interpolate in time to determine the channel response throughout the whole resource grid.

First, the pilot signals from the first two OFDM symbols (subframes 0 and 5) are combined. Instead of a separation of six subcarriers between CSR signals, this produces a

separation of three subcarriers. Then the values along the frequency axis are interpolated. Finally, the same channel response is applied to all of the OFDM symbols of the slot or subframe to find the channel response of the whole grid. Table 4.8 lists the required inputs and output obtained.

**Table 4.8** Interpolation Function

<b>SL NO</b>	<b>FUNCTION INPUT PARAMETERS</b>	<b>FUNCTION OUTPUT</b>
1	OFDM Received Symbols	Channel Response of entire Resource Grid
2	Number of subcarriers	
3	Symbol Indexing	

#### 4.7.2 Equalizer Gain Computation

A frequency-domain equalizer computes a gain for application to all received resource elements at each subcarrier. A variety of algorithms are used for frequency-domain equalization. The simplest is the Zero-Forcing algorithm, in which the gain is expressed as a ratio of the transmitted resource element and the channel response estimate at each subcarrier. A more advanced algorithm is the MMSE estimation, which requires a detailed knowledge of the channel characteristics and calculates the gain as a modified ratio that takes the effect of the uncorrelated noise of the channel into account. Following the calculation of the equalizer gain, the received element is the product of the received resource element and the equalizer gain is the best estimate. Both the algorithms ZF and MMSE equalizer are implemented in the MATLAB function, (Table 4.9) the equalization mode for which a choice can be made. The Equalised Resource Grid is shown in Fig. 4.9, and thus successfully verified.

**Table 4.9** Equalizer Gain Computation

<b>SL NO</b>	<b>FUNCTION INPUT PARAMETERS</b>	<b>FUNCTION OUTPUT</b>
1	Estimated Channel Response	Equalized Resource Grid
2	PDSCH Structure	
3	Equalization Mode	

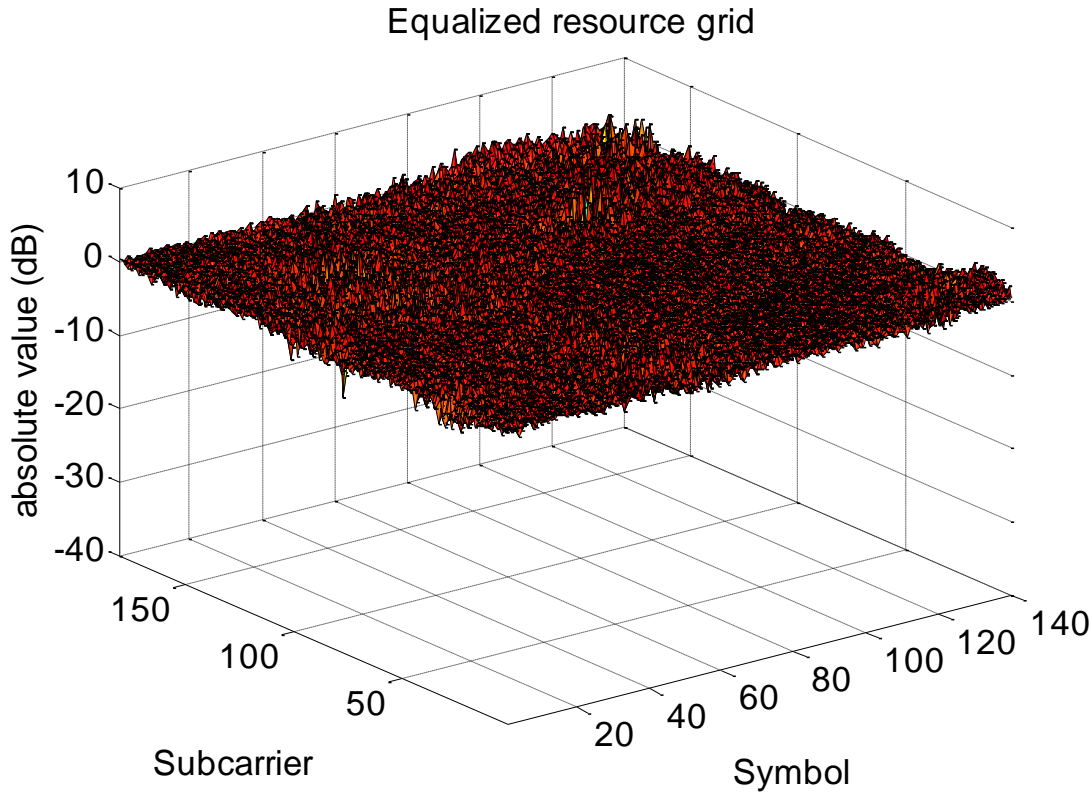


**Fig. 4.9** Equalized Resource Grid

#### 4.8 Summary

With this Chapter, Pilot-based OFDM Channel estimation, the upper portion of the Block Diagram represented by dashes in Fig. 4.10 has been successfully completed. The input signal was successfully estimated at the receiver. In the next Chapter, the remaining three blocks will be dealt with, which covers Path Loss Modeling, Power Allocation and Adaptive Beamforming.

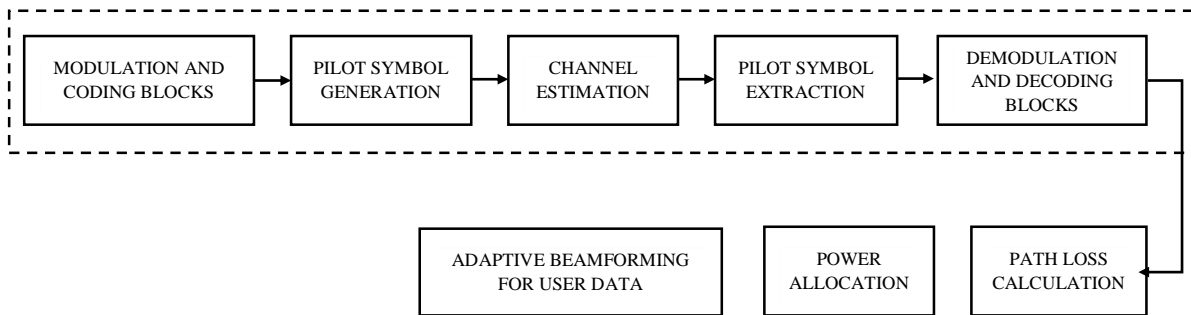


**Fig. 4.10** Completed Blocks

*Chapter 5*  
*Power Allocation and Beamforming*

## CHAPTER 5

### POWER ALLOCATION AND ADAPTIVE BEAMFORMING

This chapter contains the Core blocks, whose working is organized as follows. Section 5.1 introduces Path Loss Modeling, which helps in calculating the distance from eNodeB to UE, depending on channel conditions taken from the previous chapter. Distance based power Control is done in Section 5.2 to allocate power to UEs based on the distance evaluated by the preceding section. On power allocation, user data can now be transmitted to the UEs through LMS Adaptive Beamforming, which is dealt with in Section 5.3.

#### **5.1 Path Loss Modeling**

Path loss (PL) is the power reduction of a signal as it traverses through a medium, typically space. It is a major challenge in wireless communication and is the main factor for depicting the quality of the radio channel and hence it can be used as a controlling factor for evaluating the performance of wireless communication system to achieve the perfect network planning. There are many reasons for the attenuation of a signal as it passes through a channel between the radio transmitter and a receiver. The factors can be classified as follows:

1. Loss in the free-space, reflection, refraction, absorption and diffraction.
2. Terrain outline, type of environment (rural, semi-urban, urban, vegetation and foliage)
3. Distance between the transmitter and the receiver, height and location of antennas
4. Condition of the propagation medium (dry or moist air)

Path loss is given by,

$$PL \text{ (dB)} = 10 \log(P_t / P_r) \quad (5.1)$$

where  $P_t$  and  $P_r$  are the transmitted and received power, respectively.

##### **5.1.1 Free space equations**

In free space, the receiver (UE) antenna power, separated by distance  $d$  from the transmitter (eNodeB), is given by the Friis transmission equation:

$$P_r = \frac{P_t G_t G_r \lambda^2}{4\pi^2 d^2 L} \quad (5.2)$$

Where:  $G_t, G_r$  - transmitter, receiver antenna gains, respectively

$L$  - System loss factor

$\lambda$  - Wavelength (m)

### 5.1.2 Wireless medium equations

Equation (2) does not hold for  $d = 0$ . Hence, many propagation models use different representation for a close-in distance ( $d_0$ ), known as the received-power reference point. This is typically chosen to be 1 m. Free space is not the appropriate medium in realistic mobile radio channels. A general PL model uses a parameter  $\gamma$  to denote the power-law relationship between the separation distance and the received power. So, path loss (in decibels) for distance  $d$  can be expressed as

$$PL(d) = PL(d_0) + 10 \gamma \log(d/d_0) + X_\sigma \quad (5.3)$$

where  $\gamma = 2$  is for free space medium, and is higher for wireless environment.  $X_\sigma$  denotes a Gaussian random variable, where  $\sigma$  is the standard deviation which depicts the received power variation.

In order to find the path loss in different conditions of communication channel, propagation models can be used. Propagation model are very helpful in predicting the signal attenuation or path loss in the communication channel between the transmitter and receiver. There are 3 kinds of path loss models:

1. Empirical or statistical model - based on measured data, it is simple and uses basic statistics.
2. Semi-deterministic model – A combination of empirical as well as deterministic.
3. Deterministic/Physical model - this model is site-specific, and needs detailed information about the site geometry. The results are very high and accurate

Okumura Hata model has been used in our project, as it is the right model for simulation purposes.

### 5.1.3 Okumura Hata model

Hata model is an empirical model and it was built for three modes - urban, suburban and open areas. The model for urban areas was built first and used as the base for others.

**Table 5.1** Valid parameters range of the Okumura Hata model

Frequency ( $f_c$ )	150 MHz - 1500 Mhz
TX height ( $h_b$ )	30 m - 200 m
RX height ( $h_m$ )	1 m - 10 m
TX - RX distance (R)	1 km - 10 km

3 types of prediction area:

- Open area: Free space, no presence of tall buildings and trees in the path.
- Suburban area: highways scattered with houses and trees, village areas, and few obstacles near the mobile equipment but not very congested.
- Urban area: Big town with tall buildings and houses, well-built city, village with close houses and tall obstacles.

Empirical formulas of Okumura Hata

- Urban areas:  $PL (dB) = A + B \log_{10} R - E$
- Suburban areas:  $PL (dB) = B \log_{10} R - C$
- Open areas:  $PL (dB) = A + B \log_{10} R - D$

Where:  $A = 69.55 + 26.16 \log_{10} f_c - 13.82 \log_{10} h_b$

$$B = 44.9 - 6.55 \log_{10} h_b$$

$$C = 2 (\log_{10} (f_c/28))^2 + 5.4$$

$$D = 4.78 (\log_{10} f_c)^2 + 18.33 \log_{10} f_c + 40.94$$

$$E = 3.2 (\log_{10}(11.754 h_m))^2 - 4.97 \quad \text{for large cities, } f_c \geq 300\text{MHz}$$

$$E = (1.1 \log_{10} f_c - 0.7) h_m - (1.56 \log_{10} f_c - 0.8) \quad \text{for medium to small cities}$$

Where:

$h_m$ : Height of the user equipment antenna above local region height [m]

$h_b$ : Height of the base station antenna above local region height [m]

$R$ : Distance between user equipment and the base station [km]

$f_c$ : Frequency of the carrier signal [MHz]

$\lambda$ : Wavelength in free-space [m]

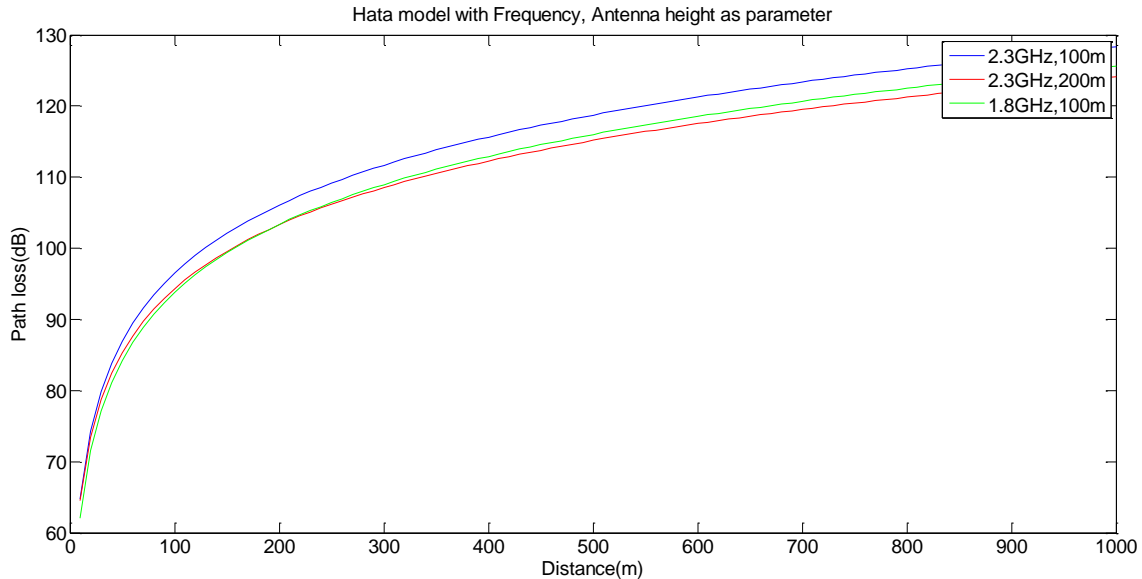


**Fig. 5.1** Okumura Hata Model

#### 5.1.4 Path Loss Model for LTE

Okumura-Hata model has been extended to cover 1.5 GHz to 2 GHz (Cost 231-Hata model)

$$PL \text{ (dB)} = F + B \log_{10} R - E + G \quad (5.4)$$

Where:  $F = 46.3 + 33.9 \log_{10} f_c - 13.82 \log_{10} h_b$

$G= 0$  dB for medium sized cities and suburban areas, and 3 dB for metropolitan areas.

The project discussion will be on an urban environment, with operating frequency, and transmission antenna height as parameters. Fig. 5.1, Fig. 5.2 illustrate the Path Loss in dB versus distance between eNodeB and UE using Okumura-Hata model, and its application to LTE respectively.

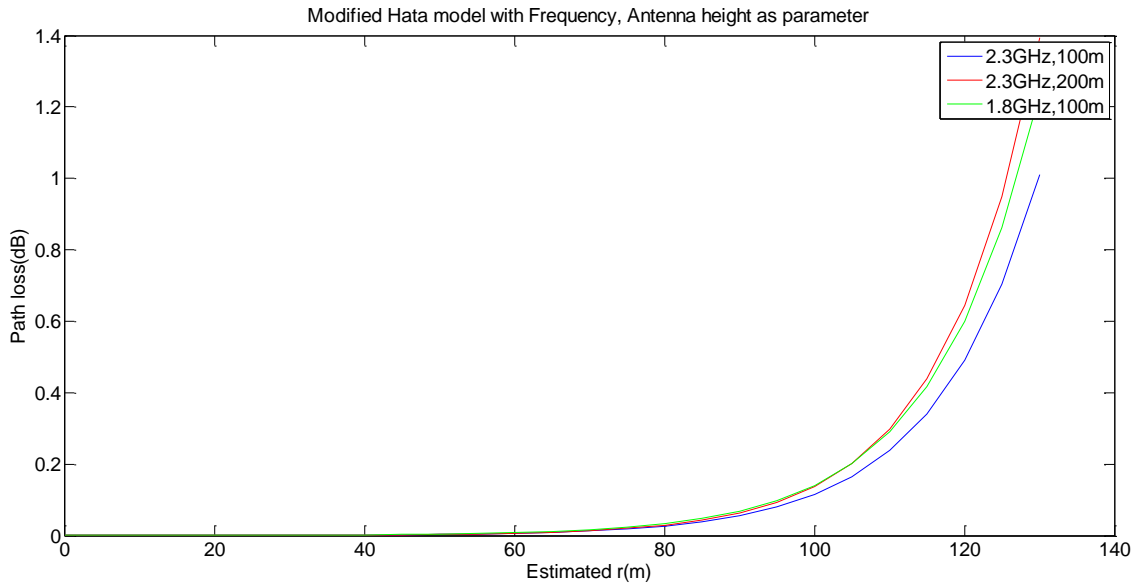


**Fig. 5.2** Okumura Hata Model for LTE

## 5.2 Power Control

Radio resource management is the system level approach to control the co-channel interference and other radio characteristics of wireless communication systems. The objective of power control is to utilize the limited radio resources to the maximum and network infrastructure as judiciously as possible. The performance and system capacity are adversely degraded by interference. Hence, power control plays a critical role in mitigating the adjacent and co-channel interference in the system and thus increasing the efficiency.

Power control is about controlling the power both in downlink and uplink. Transmitting the signal with least possible power level is the purpose of the power control. To provide the agreed Quality of Service (QoS), power of each TX is adjusted to the required level. Because of dynamic variation of the radio channel, finding the power of transmitter is a tough task. The received power should be of adequate level irrespective of the radio channel.

### 5.2.1 Distance Based Power allocation algorithm

The distance between eNodeB and UE to allocate transmitted power to each of its served mobile station is used by the algorithm. Since there is no feedback provided, it is an open-loop power control mechanism.

If power control is not employed, i.e., the transmitted power is uniform throughout its range for all users, the user at the cell edge will have the least value of the signal-to-interference ratio (SIR). Thus, the transmitted power to be allocated should be more to the mobile stations that are far from base stations.

The Distance Based Power Allocation algorithm calculates the transmitted power for each mobile m using the following equation:

$$p_m = kx_{a_m m}^n \quad (5.5)$$

$$x_{a_m m} = d_{a_m m}/R \quad \text{if } d_{a_m m} > d_{\min}$$

$$x_{a_m m} = d_{\min}/R \quad \text{if } d_{a_m m} < d_{\min}$$

k = Positive constant

n = Real positive value

R = Maximum base to mobile distance

$d_{a_m m}$  = Distance between mobile m and its assigned base station

The pseudo-code for the simulation is as follows.

#### Pseudo-code

1. Initialize number of iterations
2. Initialize number of mobiles
3. Initialize  $d_{\min}$ , R, k, n
4. for  $i = 1$  to iterations
  - Generate uniformly distributed vector of mobile-to-base station distance
  - Initialize power
  - for  $j = 1$  to mobiles
  - if  $d_{am} \leq d_{\min}$
  - $p_m(j) = k (d_{\min}/ R)^n$
  - else
  - $p_m(j) = k(d_{am}(j)/R)^n$
  - end
  - calculate SIR<sub>observed(j)</sub> and compute outage
  - end

5. Calculate the outage percentage using the outage counter and the number of mobiles.
6. Plot outage percentage versus mobiles

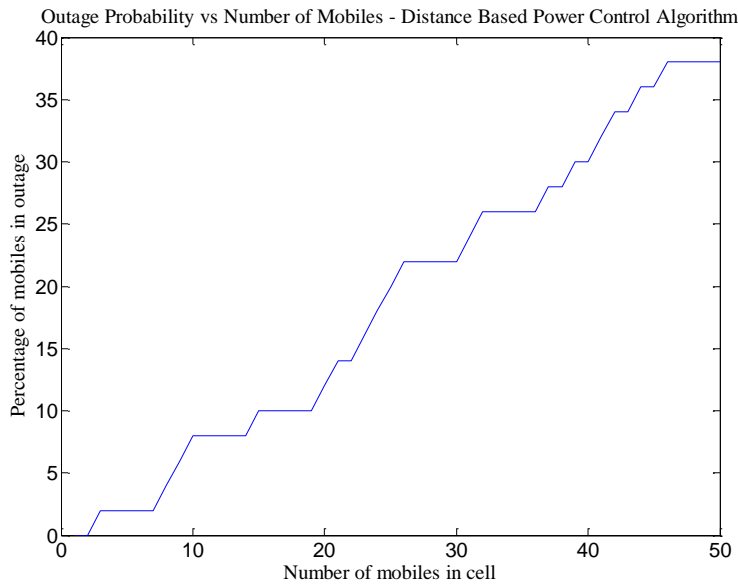


**Fig. 5.3** Outage Percentage of Mobiles in Outage versus No .of Mobiles in Cell

### 5.2.2 Power Control in LTE

The eNodeB calculates the transmit Energy for the downlink Per Resource Element (EPRE). The UE assumes that cell-specific reference-signal EPRE (RS-EPRE) is constant throughout all the downlink system bandwidth and all sub-frames until cell-specific RS power information is received. The downlink reference-signal transmit power is used to derive the cell specific reference signal which is given by the parameter reference-signal power. The reference signal downlink transmit power can be defined as the average of all the power contributions, of all resource elements in resource grid carrying the reference signals within the bandwidth. Fig. 5.3 plots the outage percentage against the number of mobiles.

The UE may assume that for 16 QAM, 64 QAM, spatial multiplexing with more than one layer, if UE-specific RSs are present in the physical resource blocks (PRBs) upon which the corresponding PDSCH is mapped, the ratio of PDSCH EPRE to UE-specific RS-EPRE within each OFDM symbol containing UE-specific RSs shall be a constant, and that constant shall be maintained over all the OFDM symbols containing the UE-specific RSs in the corresponding PRBs.

### 5.2.3 Downlink Power Allocation

A single cellular system consisting of a single eNodeB and M UEs. Each UE has a Channel Quality Indicator, CQI based on its location in the cell, where the UE near to the eNodeB has a higher CQI. Shown in Table I, higher CQI corresponds to higher modulation. Our goal is to generate different utility functions with respect to CQI values to represent the QoS of users and optimally allocate powers to UEs. The total power at eNodeB is  $P_t$ .

### 5.2.4 Mapping CQI, SNR with distance

CQI is the feedback that the UE sends to indicate the data rate which can be supported by the downlink channel. The eNodeB selects an appropriate modulation scheme and code rate for downlink transmission based on CQI values. In addition to indicating the downlink channel quality, CQI also accounts for the capabilities of the UE's receiver. Table shows the corresponding modulation scheme, code rate and efficiency for different CQI values.

A linear function has been proposed to map SNR to CQI. Then after flooring, the CQIs, obtained by the linear function (1), over all resource blocks (RB) are reported back to the eNodeB.

$$\text{CQI} = 0.5223 \text{ SNR} + 4.6176 \quad (5.6)$$

The simulated cell network has 1 eNodeB and M UEs where  $M = 15$ . The total power  $P_t$  at the eNodeB is 40W which is a typical value for macro cell base station at the antenna connector. 15 UEs are placed at different locations in the cell and one UE in each CQI zone, as seen in Fig. 5.4.

The UEs are placed at the further edge of each CQI zone, which is the worst channel quality in each CQI zone. The mapping among CQI, SNR and distance is plotted in Fig. 5.5. As the UE moves further away the CQI decreases and so as SNR. The UEs, standing in the range between 1m and 69.14m away from the eNodeB, have the best channel quality (CQI = 15) with 64-QAM. Whereas the CQI zone for the worst channel quality (CQI = 1) is 355.5m to 403.2m away from the eNodeB. Table 5.1 shows the variation of Modulation mode, efficiency with CQI.

**Table 5.2 CQI Index**

CQI Index	Modulation	Code Rate X 1024	Efficiency
0	No transmission		
1	QPSK	78	0.1523
2	QPSK	120	0.2344
3	QPSK	193	0.3880
4	QPSK	308	0.6016
5	QPSK	449	0.8770
6	QPSK	602	1.1758
7	16QAM	378	1.4766
8	16QAM	490	1.9141
9	16QAM	616	2.4063
10	64QAM	466	2.7305
11	64QAM	567	3.3223
12	64QAM	666	3.9023
13	64QAM	722	4.5234
14	64QAM	873	5.1152
15	64QAM	948	5.5547

For UE with CQI 15, the power that required to achieve the minimum QoS is about 5.22W whereas the UE with CQI 1 needs 23.24W to have the minimum QoS. A similar approach is incorporated for the modulation scheme, with a lower CQI index having QPSK at the modulator stage, and a higher index having QAM modulator.

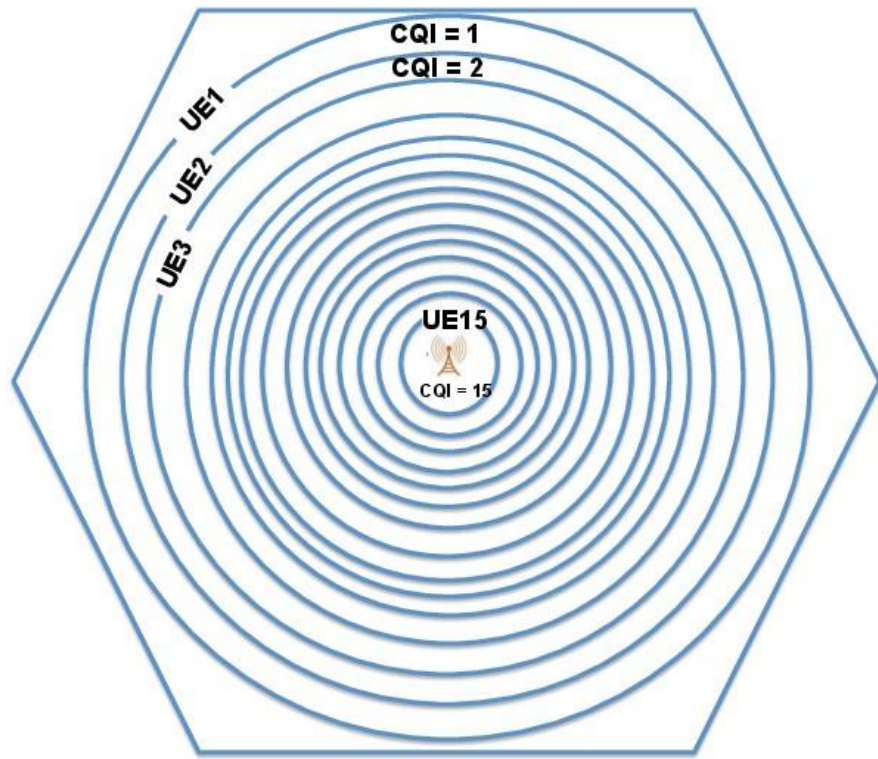


**Fig. 5.4** Simulation for eNodeB = 1 and UE = 5

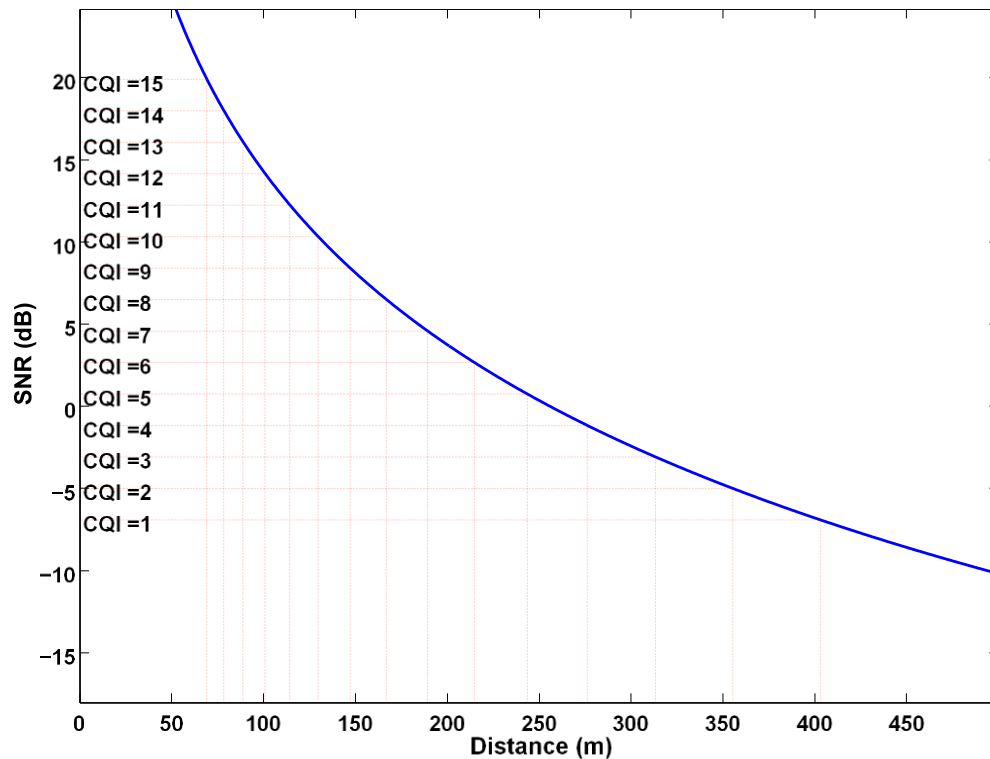


**Fig. 5.5** Mapping CQI, SNR with distance to eNodeB

### 5.3 LMS Adaptive Beamforming

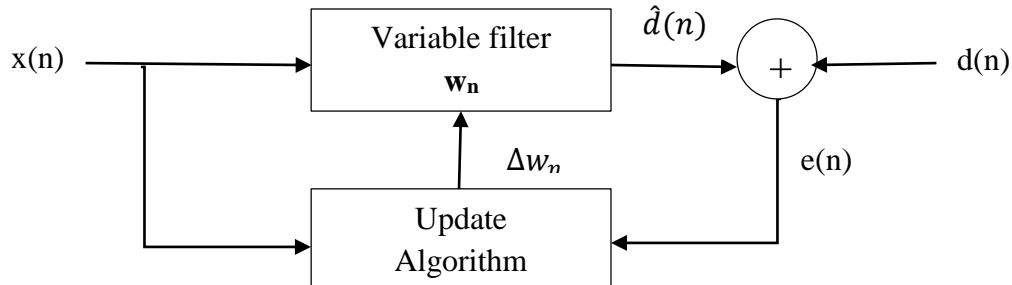


**Fig. 5.6** LMS Algorithm

Adaptive arrays allow the antenna to steer the beam to any direction of interest, while simultaneously mitigating the interfering signals. The adaptive array antenna systems make use of sophisticated array signal processing algorithms to distinguish between desired, interfering and multipath signals. These array signal processing algorithms update the array weights by determining the Direction of Arrival (DOA) of a signal and for achieving beamforming in real time. There are primarily two types of adaptive beamforming: blind and non-blind.

The LMS algorithm is a non-blind technique that can be considered to be the most common adaptive algorithm for continuous adaptation. It uses the steepest-descent method to recursively compute and update the weight vector. Owing to the steepest-descent, the updated vector will propagate to the vector which causes the least mean square error (MSE) between the beamformer output and the reference signal. The LMS algorithm can be obtained as follows.

The MSE is defined by:

$$\varepsilon^2(t) = [d^*(t) - w^H x(t)]^2 \quad (5.7)$$

$d^*(t)$  is the complex conjugate of the desired signal. The signal  $x(t)$  is the received signal from the antenna elements, and  $w^H x(t)$  is the output of the beamform antenna and  $(.)^H$  is the Hermitian operator. The expected value of both sides leads to:

$$E\{\varepsilon^2(t)\} = E\{d^2(t)\} - 2w^H r + w^H R w \quad (5.8)$$

In this relation the  $r$  and  $R$  are defined by:

$$r = E\{d^*(t)x(t)\}$$

$$R = E\{x(t)x^H(t)\}$$

$R$  is referred to as the covariance matrix. If the gradient of the weight vector  $w$  is zero, the MSE is at its minimum. This leads to:

$$\nabla_w(E\{\varepsilon^2(t)\}) = -2r + 2Rw = 0$$

The solution is called the Wiener-Hopf equation for the optimum Wiener solution:

$$w_{opt} = R^{-1}r \quad (5.9)$$

The LMS algorithm converges to this optimum Wiener solution. The basic iteration is based on the following simple recursive relation:

$$w(n+1) = w(n) + \frac{1}{2}\mu(-\nabla(E\{\varepsilon^2\})) \quad (5.10)$$

Combining equations 8, 9 and 10 gives:

$$w(n+1) = w(n) + \mu(r - R w(n))$$

The measurement of the gradient vector is not possible, and therefore the instantaneous estimate is used:

$$\begin{aligned} \hat{R}(n) &= x(n)x^H(n) \\ \hat{r}(n) &= d^*(n)x(n) \end{aligned}$$

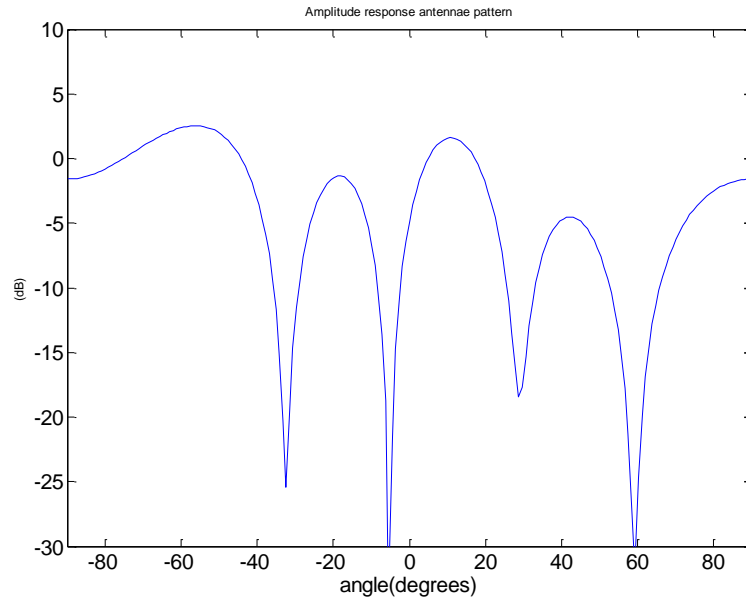
By rewriting (10) using the instantaneous estimates, the LMS algorithm can be written in its final form (11)

$$\begin{aligned} \hat{w}(n+1) &= \hat{w}(n) + \mu x(n)(d^*(n) - x^H(n)\hat{w}(n)) \\ &= \hat{w}(n) + \mu x(n)\varepsilon^*(n) \end{aligned} \quad (5.11)$$

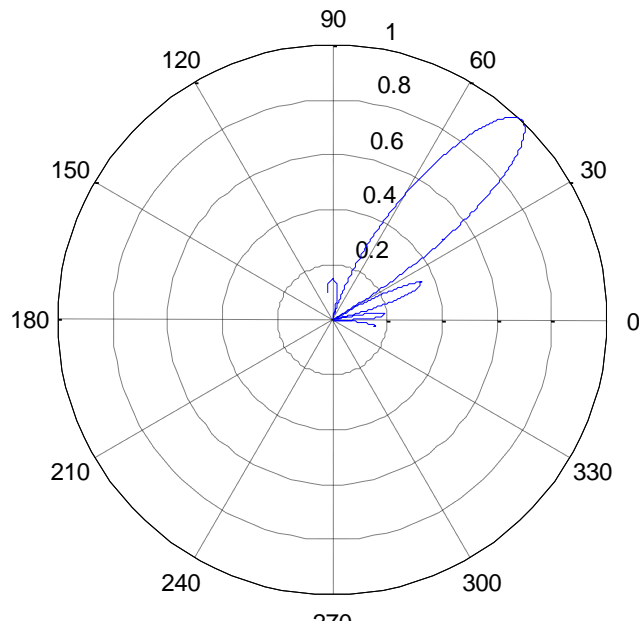
Antenna Array Pattern – For  $n$  arrays, separated by a uniform distance  $d$ , oriented at angle  $\theta$ , having weights  $w_n$ , Array Factor (AF) is given as:

$$AF(\theta) = \sum_{i=0}^{N-1} w_n e^{jkn d \sin(\theta)} \quad (5.12)$$

A MATLAB script was written for implementing LMS Algorithm, whose parameters were:  $\mu=0.05$ , angle of arrivals of desired signal is 45 degrees (Maximise Power), and interferer signals at 30, 60 degrees (Steer Nulls). Fig. 5.7, Fig. 5.8 illustrate the amplitude and polar patterns of the output, the directivity of which improves with increase in number of antennas in the array.



A



B

**Fig. 5.7 A - Amplitude pattern, B – Polar Pattern for 5 antenna system**

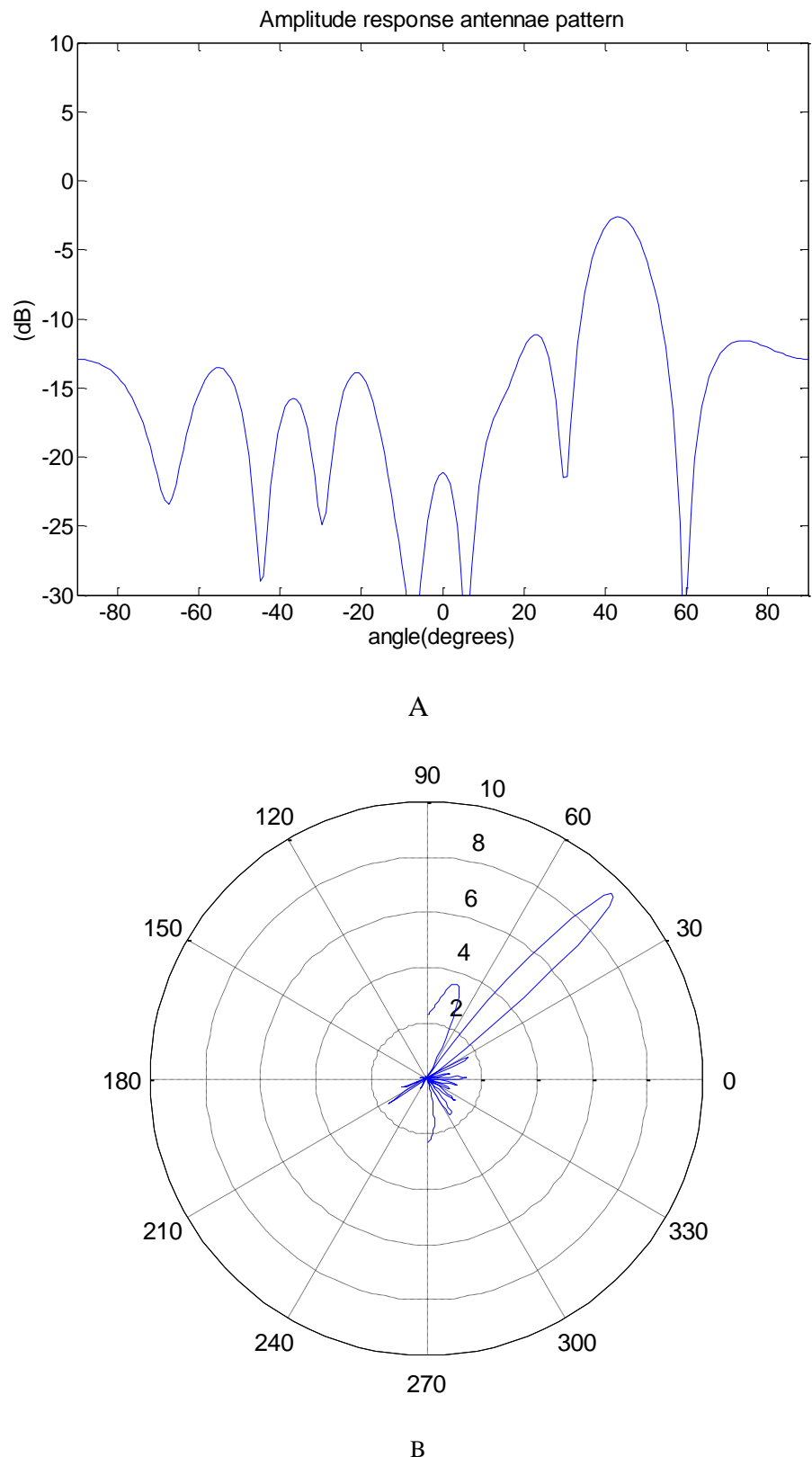


**Fig. 5.8** Same Parameter values with number of antennas increased from 5 to 10

## 5.4 Summary

In this chapter, path loss has been modelled using Okamura-Hata model to determine the distance between the user location and base station. The Matlab plots are obtained for different frequencies and base station antenna heights.

Distance based power allocation algorithm is simulated and power is allocated to the user equipments adaptively based on their radial distance from base station. The relationship between CQI, SNR and distance is used to allocate power.

Finally, LMS beamforming algorithm is simulated for uniform linear antenna arrays . The algorithm forms a beam pattern with major lobe directed towards the desired user and nulls directed towards interferers. The directivity of the beam increases with increase in the number of antenna array elements.

*Chapter 6*

*Conclusion*

## CHAPTER 6

### CONCLUSION

#### **6.1 Work Done**

The project involved design and implementation of an LTE-PHY Downlink channel at a specific stage of mobile communication that involves allocating power and adaptively beamforming the signal based on user location.

The overall schematic design used in the project was primarily composed of three parts. The LTE PHY blocks performed AWGN Modulation and Coding, which included adaptive Modulator and Demodulator, Scrambler and Descrambler to minimize interference effects, Turbo encoder and decoder for improved accuracy, Rate Matcher and Dematcher for link adaptation, CRC Generator and Detector for early termination, Codeword Re-constructor, Channel Coding and Decoding. BER vs SNR plots were simulated at each stage for performance evaluation. The second part introduced a realistic multipath fading channel to perform Pilot-based Channel Estimation. Resource Block Configuration, Pilot Generation, Resource Element Mapping and Demapping, OFDM Modulation and Demodulation, Interpolation and Equalisation were the modules involved. The two parts together contributed in forming an ‘LTE-PHY Pilot-based Channel Estimation’ module, as per LTE Standards. The final part contained Okumura-Hata based Path Loss Modeling for evaluating user distance, Distance based Power Allocation in a multi-user environment, and employing LMS Adaptive Beamforming to steer the signal towards the user location. Each block was separately implemented in MATLAB, and the performance successfully verified.

#### **6.2 Future Scope**

Out of the five enabling technologies of LTE, the ones that require further attention in terms of algorithm writing and implementation are MIMO and Link Adaptation. With these, the integrated algorithm will possess capacity to adapt to channel quality, different modulation and coding techniques, number of transmit or receive antennas, and transmission bandwidth. After channel-dependent scheduling, a Simulink model can be constructed for the complete block.

The algorithms need to be converted to optimized C codes and must be implemented on the TI DSP Platform. Hardware implementation and verification will enhance the proximity of the project to real mobile communication scenario.

### **6.3 Learnings from the Project**

The team has had the following value additions during the tenure of this project:

1. We have gained a thorough understanding of the fundamentals of LTE-PHY and its downlink algorithms, coding and simulation of each block in modern tool MATLAB 2014a.
2. The major outcome of the project has been to understand the applications of Smart Antennas, Adaptive Beamforming, Path Loss Modeling, and Power Control in LTE.
3. The literature survey carried out during the project led to the understanding of the historical development of wireless technologies, beam forming algorithms and adaptive modulation.
4. During the course of project there has been a huge exposure to a number of quality research work, referred from IEEE transaction papers, published by researchers from esteemed universities around the globe. This exposure led to the understanding of current research trend and paved way to venture into the mathematical intricacies of the various signal processing algorithms.
5. Another outcome from the project has been in learning the simulation on MATLAB, using system objects and toolboxes. We were introduced to various opportunities and research activities in the field of LTE systems, thus strengthening the Engineering background of Signal Processing.
6. On a broader scope, the project helped in building team relationship, time management and working coherently in a group with proper communication. It also helped in gaining confidence for presentation and report writing skills.

## REFERENCES

1. H. Zarrinkoub, "Understanding LTE with MATLAB: From mathematical modeling to simulation and prototyping". John Wiley & Sons, 2014. ISBN: 978-1-1184-4341-5
2. J. W. Mink, H. S. Hwang, C. W. Hicks, T. W. Nuteson, M. B. Steer, J. Harvey, "Spatial power combining for two dimensional structures" Millimeter Waves, 1997 Topical Symposium on, 1997, pp. 133-136.
3. B. L. Ng, Y. Kim, J. Lee, Y. Li, Y. H. Nam, J. Zhang, K. Sayana, "Fulfilling the promise of massive MIMO with 2D active antenna array", IEEE Globecom Workshops, pp. 691-696, 2012.
4. Y. Zhu, Y. L. Liu, A. Wang, K. Sayana, J. C. Zhang, "DoA estimation and capacity analysis for 2D active massive MIMO systems", IEEE International Conference on Communications (ICC), pp. 4630-4634, 2013.
5. Y. Hashimoto, Y. Fujino, Y. Kuwahara, "Orthogonal coding for the pilot symbol of MMSE adaptive antenna for W-CDMA reverse link", IEEE Region 10 Conference, Vol. 1, pp. 499-502, 2004.
6. A. Seeger, M. Sikora, W. Utschick, "Antenna weight verification for closed-loop downlink Eigen beam forming", Global Telecommunications Conference, GLOBECOM '02. IEEE, Vol. 1, pp. 982-986, 2002.
7. S. Nagaraj, Yih-Fang Huang, "Multiple antenna transmission with channel state information: a low-rate feedback approach", IEEE Signal Processing Letters, Vol. 11, pp. 573-576, 2004.
8. A. Maaref, S. Aissa, "Generalized Performance Analysis of Adaptive PSAM-Based Transmit-Beamforming for Wireless MIMO systems", IEEE 63rd Vehicular Technology Conference, Vol. 5, pp. 2578-2582, 2006.
9. Gang Jin, Yanjun Hu, "A Novel Channel Estimation based on Pilot-Aided in LTE Downlink Systems", Seventh International Symposium on Computational Intelligence and Design (ISCID), Vol. 2, pp. 424-428, 2014.
10. Tareq Y. Al-Naffouri, K. M. Zahidul Islam, Naofal Al-Dhahir, Sili Lu, "A Model Reduction Approach for OFDM Channel estimation Under High Mobility Conditions" , vol. 58, pp. 2181-2193, 2010.

11. Yang Qin, Bing Hui, KyungHi Chang, “Performance and complexity evaluation of pilot-based channel estimation algorithms for 3GPP LTE downlink”, Second International Conference on Ubiquitous and Future Networks (ICUFN), pp. 218-221, 2010.
12. Johanna Ketonen, Markku Juntti, Jari Ylioinas, Joseph R. Cavallaro, “Implementation of LS, MMSE and SAGE channel estimators for mobile MIMO-OFDM”, Conference Record of the Forty Sixth Asilomar Conference on Signals, Systems and Computers (ASILOMAR), pp. 1092-1096, 2012.
13. Meilong Jiang, Guosen Yue, Narayan Prasad, Sampath Rangarajan, “Enhanced DFT-Based Channel Estimation for LTE Uplink”, Vehicular Technology Conference (VTC Spring), IEEE 75th, pp. 1-5, 2012.
14. Fanghua Weng, Changchuan Yin, Tao Luo, “Channel estimation for the downlink of 3GPP-LTE systems”, 2nd IEEE International Conference on Network Infrastructure and Digital Content, pp. 1042-1046, 2010.
15. Won Jun Hwang, Jun Hee Jang, Hyung Jin Choi, “An enhanced channel estimation method for MU-MIMO based LTE-Advanced system”, 17th Asia Pacific Conference on Communications, pp. 163-167, 2011.
16. Wei Guo, Guojin Li, “Study on channel estimation of Long Term Evolution”, IEEE 3rd International Conference on Communication Software and Networks (ICCSN), pp.367 – 369, 2011.
17. Manda Rajarao, R V Raja Kumar, Divya Madhuri, Madhavi Latha, “Efficient channel estimation technique for LTE air interface”, Asia Pacific Conference on Postgraduate Research in microelectronics and electronics”, pp. 214-219, 2012
18. Sung-Hyuk Shin, Chang-Soo Koo, D. Grieco, A. Zeira, “Pathloss-aided closed loop transmit power control for 3G UTRA TDD”, The 57th IEEE Semiannual Vehicular Technology Conference, VTC 2003-Spring, Vol. 4, pp. 2226-2230, 2003.
19. Bilal Muhammad, Abbas Mohammed, “Uplink closed loop power control for LTE system”, 6th International Conference on Emerging Technologies (ICET), pp. 88-93, 2010.

20. Manda Rajarao, R V Raja Kumar, Divya Madhuri, Madhavi Latha, “Efficient channel estimation technique for LTE air interface”, Asia Pacific Conference on Postgraduate Research in microelectronics and electronics, pp. 214-219, 2012.
21. Sung-Hyuk Shin, Chang-Soo Koo, D. Grieco, A. Zeira, “Pathloss-aided closed loop transmit power control for 3G UTRA TDD”, The 57th IEEE Semiannual Vehicular Technology Conference, VTC 2003-Spring, Vol. 4, pp. 2226-2230, 2003.
22. Bilal Muhammad, Abbas Mohammad, “Uplink closed loop power control for LTE system”, 6th International Conference on Emerging Technologies (ICET), pp. 88-93, 2010.
23. Chieh-Ho Lee, Chung-Ju Chang, “Performance analysis of a truncated closed-loop power-control scheme for DS/CDMA cellular systems”, IEEE Transactions on Vehicular Technology”, Vol. 53, pp. 1149-1159, 2004.
24. Hamed Saghaei, Abbas Ali Lotfi Neyestanak, “Variable Step Closed-Loop Power Control in Cellular Wireless CDMA Systems under Multipath Fading”, IEEE Pacific Rim Conference on Communications, Computers and Signal Processing, pp. 157-160, 2007.
25. R. Mullner, C. F. Ball, “Contrasting Open-Loop and Closed-Loop Power Control Performance in UTRAN LTE Uplink by UE Trace analysis”, IEEE International Conference on Communications, pp. 1-6, 2009.
26. Qinjin Chen, Hui Zhao, Lin Li, Hang Long, Jianquan Wang, Xiaoyue Hou, “A Closed-Loop UL Power Control Scheme for Interference Mitigation in Dynamic TD-LTE Systems”, IEEE 81st Vehicular Technology Conference (VTC Spring), pp. 1 - 5, 2015.
27. Arne Simonsson, Anders Furuskar, “Uplink Power Control in LTE - Overview and Performance, Subtitle: Principles and Benefits of Utilizing rather than Compensating for SINR Variations”, Vehicular Technology Conference, VTC 2008-Fall. IEEE 68th, pp. 1-5, 2008.
28. K L V Sai Prakash Sakuru, Mushunuri Visali, “Power control based resource allocation in LTE uplinks”, International Conference on Communications and Signal Processing (ICCSP), pp. 0579-0582, 2015.

29. E. M. Al-Ardi, R. M. Shubair, M. E. Al-Mualla, “Performance evaluation of the LMS adaptive beamforming algorithm usedin smart antenna systems”, IEEE 46th Midwest Symposium on Circuits and Systems, Vol. 1, pp. 432-435, 2003.
30. Ahmed El Naggary, Said El Khamy, “LTE-A edge users improvement using soft fractional frequency reuse and adaptive beam forming technique”, Middle East Conference on Antennas and Propagation (MECAP), pp. 1-5, 2012.
31. Sen Wang, Dacheng Yang, et el., “A Novel Single-/Multi-Layer Adaptive Scheme for Eigen Based Beam forming in TD-LTE Downlink”, Vehicular Technology Conference (VTC Fall), 2011 IEEE, pp. 1 – 5,2011.
32. DSP System Toolbox, MathWorks.
33. Communications System Toolbox, MathWorks.
34. 3GPP (2009) Evolved Universal Terrestrial Radio Access (E-UTRA); Multiplexing and Channel Coding. TS 36.212.
35. Y.S. Cho, J.K. Kim, W.Y. Yang, C.G. Kang, “MIMO-OFDM Wireless Communications with MATLAB”, John Wiley and Sons (Asia) Pte Ltd, 2010.
36. A. Ghosh, R. Ratasuk, “Essentials of LTE and LTE-A”, Cambridge University Press, 2011.
37. Y. Song, et el., “Investigation on elevation beam forming for future LTE-Advanced”, IEEE International Conference on Communications Workshops (ICC), pp. 106-110, 2013.
38. J. Koppenborg, H. Halbauer, S. Saur, C. Hoek, “3D beam forming trials with an active antenna array”, International ITG workshop on smart antennas (WSA),pp. 110-114, 2012.
39. Y. H. Nam, Y. Li, J. C. Zhang, “3D channel models for elevation beamforming and FD-MIMO in LTE-A and5G”, 48th Asilomar Conference on Signals, Systems and Computers, pp. 805-809, 2014.
40. T. A. Thomas and F. W. Vook, “Transparent user specific 3D MIMO in FDD using beam space methods”, IEEE Global Communications Conference (GLOBECOM), pp. 4618-4623, 2012.

41. F. W. Vook, et el., "Elevation beam forming with beam space methods for LTE", IEEE 24th Annual International Symposium on Personal, Indoor, and Mobile Radio Communications (PIMRC), pp. 554-558, 2013.
42. Y. Yuan, Y. Wang, W. Zhang, F. Peng, "Separate Horizontal and Vertical Codebook Based 3D MIMO Beamforming Scheme in LTE-A Networks", Vehicular Technology Conference (VTC Fall), IEEE 78th, pp. 1-5, 2013.
43. Y. S. Cheng and C. H. Chen, "A novel 3D beam forming scheme for LTE-Advanced system", 16th Asia-Pacific Network Operations and Management Symposium (APNOMS), pp. 1-6, 2014.

## APPENDIX – RESOURCE GRID CONFIGURATION

### A.1 Resource Grid Composition

The size and composition of the resource grid and how it is updated every subframe will be discussed. An assumption is made that the LTE transceiver processes one subframe at a time. Since the length of each subframe is 1ms, processing one second of data involves processing 1000 iterations of the transceiver. The LTE Resource Grid content is as shown earlier in Fig. 4.2.

In each subframe, the size of the resource grid ( $N_{\text{total}}$  = the total number of symbols that fill up the grid) is a function of the following four parameters:

$N_{\text{rb}}$  - Number of resource blocks in resource grid

$N_{\text{sc}}$  - Number of sub-carriers in resource blocks

$N_{\text{sym}}$  - Number of symbols per slot

$N_{\text{slot}}$  - Number of slots per subframe

The total resource grid size is the product of the number of rows, i.e. total number of subcarriers and number of columns, i.e. total number of OFDM symbols per subframe. The total number of subcarriers is the product of the number of resource blocks ( $N_{\text{rb}}$ ) and number of subcarriers per resource block ( $N_{\text{sc}}$ ). The total number of OFDM symbols per subframe is the product of the number of symbols per slot ( $N_{\text{sym}}$ ) and number of slots per subframe ( $N_{\text{slot}}$ ).

$$N_{\text{total}} = N_{\text{rb}} \times N_{\text{sc}} \times N_{\text{sym}} \times N_{\text{slot}} \quad (\text{A.1})$$

The number of slots per subframe ( $N_{\text{slot}}$ ) is a constant value of 2. The number of symbols per slot ( $N_{\text{sym}}$ ) depends on whether a normal or an extended CP is used. As throughout this book we will be using a normal CP, the number of symbols per slot will have a constant value of 7. The number of subcarriers per resource block ( $N_{\text{sc}}$ ) also depends on CP type, which has a constant value of 12 for a normal CP. Therefore, the resource grid size completely depends on the number of resource blocks, which is a direct function of the bandwidth.

## A.2 Resource Element Mapping

The Resource elements come from six types of data source: user data, CSR, DCI, PSS, SSS, and BCH. Some of these sources are available in all subframes of a frame (user data, CSR, DCI), some are only available in subframes 0 and 5 (PSS and SSS), and some are only available in subframe 0 (BCH). Since the total number of symbols in a resource grid is constant, in each frame we must compute the amount of user data in three different ways:

1. For subframe 0: Where all the sources of data are present.
2. For subframe 5: Where besides user data, CSR, DCI, PSS, and SSS are present.
3. All other subframes {1, 2, 3, 4, 6, 7, 8, 9}: Where besides user data, only CSR and DCI symbols are present.

Fig. A.1 illustrates the relative locations of six different types of data within the resource grid, with A – subframe 0, B – subframe 5, C – Remaining subframes

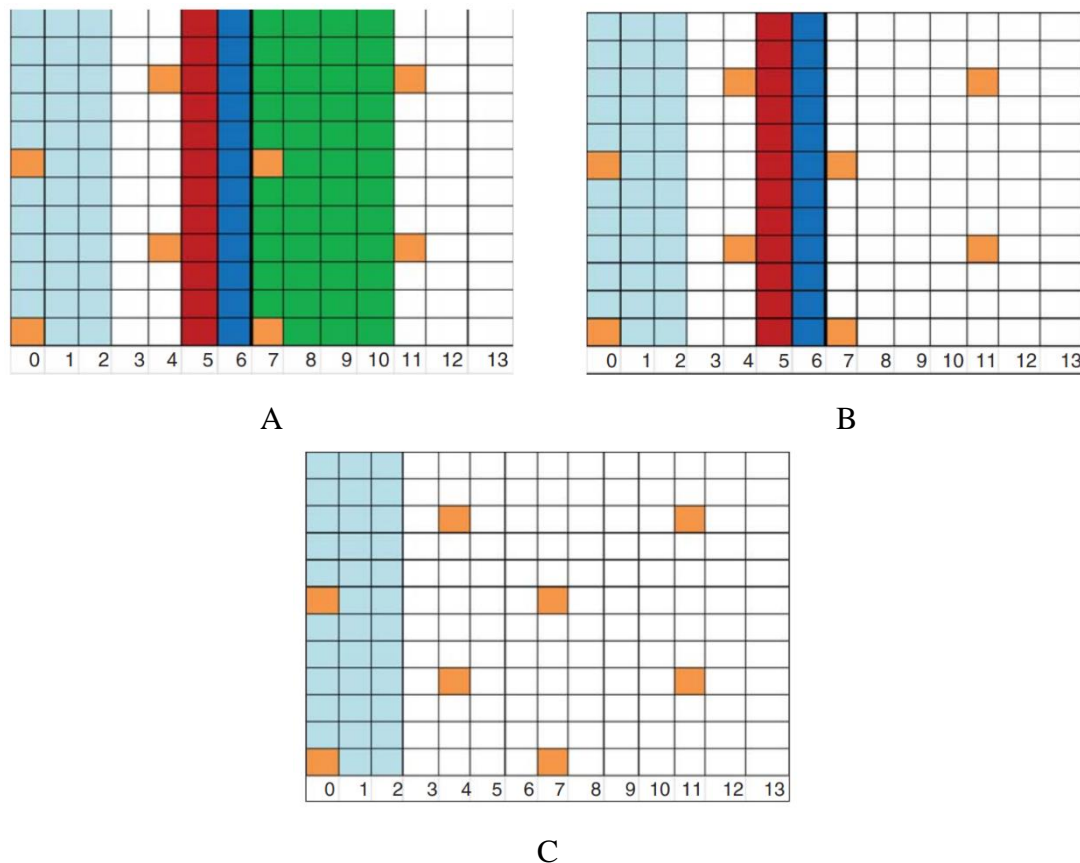


**Fig. A.1** Mapping the six data sources on the Resource Grid

If the bandwidth is constant the resource grid size is constant and is the sum of all these constituents:

$$N_{\text{total}} = N_{\text{user data}} + N_{\text{CSR}} + N_{\text{DCI}} + N_{\text{PSS}} + N_{\text{SSS}} + N_{\text{BCH}} \quad (\text{A.2})$$

### A.2.1 CSR Symbols

CSRs are placed throughout each resource block in each subframe with a specific pattern of time and frequency separations. In the single-antenna configuration, LTE specifies two CSR symbols per resource block in each of the four OFDM symbols {0, 5, 7, 12} in any subframe. In OFDM symbols 0 and 7, the starting indices are the first subcarrier, whereas in symbols 5 and 12 the starting index is the fourth subcarrier. The separation between two CSR symbols in the frequency domain is six subcarriers. There are a total of  $N_{\text{CSR}} = 8N_{\text{rb}}$  CSR symbols available in the resource grid.

### A.2.2 DCI Symbols

The DCI is placed within the first  $N$  OFDM symbols in each subframe, where  $N$  is either 1, 2, or 3. The DCI occupies all the resource elements of the first and possibly the second and third OFDM symbols in each subframe, with the exception of the CSR data. The size of the DCI per subframe is  $N_{\text{DCI}} = N_{\text{rb}} (10 + 12(N - 1))$ .

### A.2.3 BCH Symbols

The BCH is located within subframe 0 and occupies six central resource blocks from the seventh to the tenth OFDM symbol. Since the seventh OFDM symbol includes CSR symbols, its BCH has a size of only 60 ( $72 - 2 \times 6$ ), whereas in the next three symbols the size is 72. The total BCH size for the whole frame is  $N_{\text{BCH}} = 60 + 3 \times 72 = 276$ .

### A.2.4 Synchronization Symbols

The PSS occupies the sixth OFDM symbol and the SSS occupies the fifth symbol in subframes 0 and 5. The total number for each of the synchronization signals is  $N_{\text{PSS}} = N_{\text{SSS}} = 72$  per subframe, and since two subframes per frame contain synchronization signals, the total is 144 for the frame.

### A.2.5 User-Data Symbols

The total amount of data in the resource grid depends on the number of resource blocks or essentially on the bandwidth.

The presence or absence of BCH or synchronization signals in a subframe depends on the subframe index. As a result, the size of the user data in a subframe also depends on the subframe index in the following way:

1. Subframe 0: Where all sources of data are present

$$N_{\text{user data}} = N_{\text{total}} - (N_{\text{CSR}} + N_{\text{DCI}} + N_{\text{PSS}} + N_{\text{SSS}} + N_{\text{BCH}}) \quad (\text{A.3})$$

2. Subframe 5: Where besides user data, CSR, DCI, PSS, and SSS are present

$$N_{\text{user data}} = N_{\text{total}} - (N_{\text{CSR}} + N_{\text{DCI}} + N_{\text{PSS}} + N_{\text{SSS}}) \quad (\text{A.4})$$

3. All other subframes {1, 2, 3, 4, 6, 7, 8, 9}: Where besides user data, only CSR and DCI symbols are present

$$N_{\text{user data}} = N_{\text{total}} - (N_{\text{CSR}} + N_{\text{DCI}}) \quad (\text{A.5})$$